Available online at www.sciencedirect.com

SciVerse ScienceDirect

journal homepage: www.elsevier.com/locate/he

Influence of N_2 concentration in a CH_4/N_2 dielectric barrier discharge used for CH_4 conversion into H_2

Ramses Snoeckx [a,*], *Mahsa Setareh* [a,b,**], *Robby Aerts* [a], *Peter Simon* [a], *Ali Maghari* [b], *Annemie Bogaerts* [a]

[a] *Department of Chemistry, Research Group PLASMANT, University of Antwerp, Universiteitsplein 1, 2610 Wilrijk, Belgium*

[b] *Department of Physical Chemistry, School of Chemistry, College of Science, University of Tehran, Tehran, Iran*

ARTICLE INFO

Article history:
Received 3 June 2013
Received in revised form
13 September 2013
Accepted 22 September 2013
Available online 23 October 2013

Keywords:
Dielectric barrier discharge
Experiment
Simulations
Methane/nitrogen
Hydrogen
Nitrogen metastable states

ABSTRACT

We present a combined study of experimental and computational work for a dielectric barrier discharge (DBD) used for CH_4 conversion into H_2. More specifically, we investigated the influence of N_2 as an impurity (1–50,000 ppm) and as additive gas (1–99%) on the CH_4 conversion and H_2 yield. For this purpose, a zero-dimensional chemical kinetics model is applied to study the plasma chemistry. The calculated conversions and yields for various gas mixing ratios are compared to the obtained experimental values, and good agreement is achieved. The study reveals the significance of the $N_2(A^3\sum_u^+)$ and $N_2(a'^1\sum_u^-)$ metastable states for the CH_4 conversion into H_2, based on a kinetic analysis of the reaction chemistry.

1. Introduction

Natural gas is a mixture of several hydrocarbons belonging to the paraffin series (at least 95%) and non-hydrocarbon gases such as nitrogen (up to 5%), carbon dioxide and hydrogen sulfide. Methane is the principal component (between 70 and 90%) of most natural gas reserves [1,2]. The composition of natural gas varies significantly depending on the geographical source, time of year, and treatments applied during production or transportation [3]. In many respects methane is an attractive fuel for heating and electrical power generation. However, this makes methane an underutilized source for the production of valuable and useful chemicals and liquid fuels, such as hydrogen gas, higher hydrocarbons, syngas (a mixture of CO and H_2), methanol (CH_3OH) and formaldehyde (CH_2O). Both methane itself and carbon dioxide—derived from oxidizing methane—are greenhouse gases, and the global warming potential of methane is even 21 times higher than for carbon dioxide [4]. Development of efficient natural gas conversion technologies is therefore urgent and essential for a sustainable feedstock for the chemical industry and for protecting our environment.

* *Corresponding author*. Tel.: +32 32652382.
** *Corresponding author*. Department of Chemistry, Research Group PLASMANT, University of Antwerp, Universiteitsplein 1, 2610 Wilrijk, Belgium
E-mail addresses: ramses.snoeckx@uantwerpen.be (R. Snoeckx), mahsa.setareh@uantwerpen.be (M. Setareh).
0360-3199/$ – see front matter
http://dx.doi.org/10.1016/j.ijhydene.2013.09.136

The indirect synthesis routes for the utilization of methane require syngas as an intermediate step. The most important processes for the intermediate syngas step are steam methane reforming (SMR), dry reforming of methane (DRM) and partial oxidation of methane (POX). These processes are often followed by a methanol or Fischer-Tropsch synthesis to obtain the desired products [5]. The latter methods are, however, characterized by low overall yields and they require a high energy input [6]. Direct (thermal) synthesis routes, for the conversion of methane to desired products, have the advantage that they circumvent the expensive and energy intensive syngas step. They are currently, however, technologically very challenging and costly, while only achieving the same low yields [5].

This results in a growing interest for alternative (non-conventional) reforming processes, like plasma technology. The advantage of non-thermal plasmas is that the gas can remain near room temperature while being "activated" by electron impact excitation, ionization and dissociation reactions. Several types of plasmas have already been used for the conversion of methane [7–9], including dielectric barrier discharges (DBD) [6,10–15], microwave discharge [16,17], glow discharges [18,19], coronas [19,20], sparks [21], gliding arc plasma-jets [22–24], radio-frequency (RF) plasmas [25,26] and thermal plasmas [27]. In this paper, we focus on the conversion of methane by means of a non-thermal DBD. Ever since the application of a DBD for ozone generation by W. Siemens [28], DBDs have been frequently used for the removal and/or production of various compounds [14,28–32]. More specifically, we will investigate the effect of N_2 on the CH_4 conversion and H_2 yield, both in the ppm range, as N_2 is typically present as impurity in natural gas, as well as in the % range (1–99%), to investigate whether nitrogenated compounds can be formed, which could be of interest for the chemical industry.

Plasmas produced in N_2-hydrocarbon gas mixtures and the resulting chemical reactions between the various plasma species have attracted the attention of several researchers [23,33–40]. This is the result of various applications under study, such as cleaning of polluted air streams, plasma assisted ignition and combustion, nitrocarburizing, production of hydrogen and higher order hydrocarbon molecules and studying the atmospheric chemistry of Titan. Furthermore, a mixture with N_2 also offers more stable plasma conditions, as reported in literature [37]. In our own experiments, we also observed the discharge to be more homogenous and we were able to ignite it at lower power inputs. Especially, the influence of N_2 on the plasma chemistry and discharge characteristics is being studied [33,35–38], since the metastable states of N_2 play an important role in the dissociation of hydrocarbon molecules [23,33,34,37,41].

In this paper, we present a combined study of experiments and computer simulations to investigate the CH_4 conversion and resulting product yields, i.e. with focus on H_2, for several CH_4/N_2 mixtures in a DBD setup. Furthermore, by means of a kinetic analysis, based on the simulation results, we will elucidate the role of various plasma species, and especially of the N_2 metastable states, in the CH_4 conversion process. As mentioned above, both the effect of N_2 impurities (1–50,000 ppm) in a CH_4 discharge, as well as a CH_4/N_2 discharge with N_2 content ranging from 1 to 99%, will be studied.

2. Experimental

2.1. Plasma reactor

Fig. 1 shows a schematic diagram of the experimental setup. The experiments are carried out in a cylindrical DBD reactor, consisting of a stainless steel inner electrode and a coaxial quartz tube, which is covered by a stainless steel mesh electrode. The outer electrode is connected to a high voltage output and the inner electrode is grounded via an external capacitor (10 nF). The length of the discharge region is 90 mm and the discharge gap is fixed at 1.5 mm, resulting in a discharge volume of 21.9 cm^3 CH_4 and N_2 are used as feed gases with a constant total flow rate of 605 ml min^{-1} and N_2 content of 1, 10, 19, 29, 39, 48, 58, 67, 77 and 87%, controlled with mass flow controllers (Bronkhorst). The DBD reactor is powered by an AC high-voltage power supply (AFS), providing a maximum peak-to-peak voltage of 40 kV and a variable frequency of 1–90 kHz. The total current (I_t) is recorded by a Rogowski-type current monitor (Pearson 4100), while a high voltage probe is used to measure the applied voltage (U_a). Furthermore, to obtain the charge generated in the discharge, the voltage on the external capacitor (U_c) is measured. Finally, all the electrical signals are sampled by a four-channel digital oscilloscope (Picotech PicoScope) and for measuring the discharge power a control system is used to calculate the area of the Q-U Lissajous figures.

2.2. Product analysis

The feed and product gases are analyzed by a three-channel compact-gas chromatograph (CGC) (Interscience), equipped with two thermal conductivity detectors (TCD) and a flame ionization detector (FID). The first TCD channel contains a Molecular Sieve 5A column for the segregation of H_2, CH_4 and N_2, while the second TCD channel is equipped with a Rt-Q-BOND column for the measurement of C_2–C_4 hydrocarbons

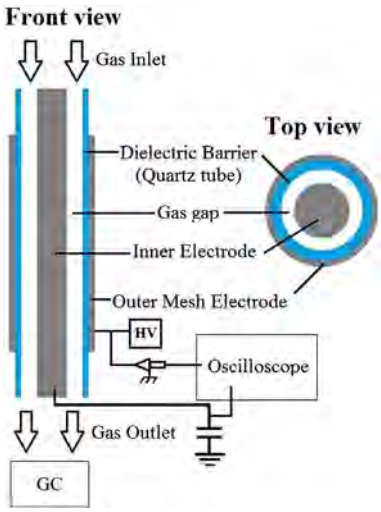

Fig. 1 – Schematic diagram of the experimental setup.

Table 1 – List of species included in the model for the CH_4/N_2 gas mixture.

Molecules	Charged species	Radicals	Excited species
CH_4	CH_5^+, CH_4^+, CH_3^+, CH_2^+, CH^+, C^+	CH_3, CH_2, CH, C	
C_2H_6, C_2H_4, C_2H_2	$C_2H_6^+$, $C_2H_5^+$, $C_2H_4^+$, $C_2H_3^+$, $C_2H_2^+$, C_2H^+, C_2^+	C_2H_5, C_2H_3, C_2H, C_2	
C_3H_8, C_3H_6		C_3H_7, C_3H_5	
C_4H_2			
H_2	H_3^+, H_2^+, H^+, H^-	H	H_2(R), H_2(V), H_2^*, H^*
N_2	N_4^+, N_3^+, N_2^+, N^+	N	N_2(R), N_2(V), $N_2(A^3\sum_u^+)$, $N_2(a'^1\sum_u^-)$, N^*
HCN	HCN^+	H_2CN, CN	
NH_3	NH_4^+, NH_3^+, NH_2^+, NH^+	NH_2, NH	NH_3^*
N_2H_4, N_2H_2		N_2H_3, N_2H	
	electrons		

and nitrogen containing compounds. The FID is equipped with a Rtx-5 column for the measurement of C_1–C_{10} and nitrogen containing compounds.

The conversion, X, of CH_4 is defined as:

$$X_{CH_4} = \frac{\text{moles of } CH_4 \text{ converted}}{\text{moles of } CH_4 \text{ input}}$$

The selectivity, S, and yield, Y, can be calculated as (illustrated here for H_2 as the major product):

$$S_{H_2} = \frac{\text{moles of } H_2 \text{ produced}}{2 \times \text{moles of } CH_4 \text{ converted}}$$

$$Y_{H_2} = \frac{\text{moles of } H_2 \text{ produced}}{2 \times \text{moles of } CH_4 \text{ input}} = X_{CH_4} \times S_{H_2}$$

It should be noted that there is also some soot and polymer deposition on the reactor walls so that the carbon and hydrogen balance is not completely 100%.

3. Description of the model

3.1. 0D chemical kinetics model

The computational model used in this work to describe the plasma chemistry is a zero-dimensional (0D) kinetic model, called Global_kin, developed by M. Kushner and coworkers [32,42]. In this model, the time-evolution of the species densities is calculated, based on the production and loss terms, as defined by the chemical reactions. The electron temperature is calculated with an energy balance equation and the rate coefficients of the electron impact reactions are a function of this electron temperature, and are calculated in a Boltzmann equation module. For a more detailed description see our previous work [10].

3.2. Plasma chemistry included in the model

The plasma chemistry used in the model is based on several chemistry sets. The hydrocarbon chemistry was developed in previous work [10], the N_2 chemistry was adopted from Van Gaens et al. [43]. Finally, these reactions were expanded with hydrocarbon-N_2 coupling reactions from literature [33,38,44]. The model considers 68 different species, including the electrons, various molecules, radicals, ions and excited species. Two types of (electronically excited) metastable N_2 species are included in the model, i.e., $N_2(A^3\sum_u^+)$ and $N_2(a'^1\sum_u^-)$. All these species are listed in Table 1. They react with each other in 598 reactions: 194 electron impact reactions, 194 ion reactions and 210 neutral reactions, which are listed in the Appendix (Tables A1,A2,A3,A4,A5, and A6), together with the corresponding rate coefficients and the references where these data are adopted from.

The carbon balance in the experiments, dropped from 97% to 89% upon rising N_2 concentration from 1% to 87%, which is in agreement with the "visual" observation that more soot/polymer was deposited on the reactor walls when increasing the N_2 content. In the simulations, carbon formation reactions are also included, but as the model is zero-dimensional, it is not possible to predict the carbon balance in an accurate way, because carbon formation and especially diffusion/deposition/accumulation appears to be most important on the reactor walls, which needs at least a one-dimensional model.

3.3. Description of the DBD setup in the model

Since the model is zero-dimensional, we can only simulate the plasma behavior as a function of time and we cannot describe the spatial variation of our cylindrical DBD reactor in a direct manner. However, the temporal behavior can be translated into a spatial behavior (i.e., as a function of distance along the DBD tube) by means of the gas flow (i.e., similarity between batch reactor and plug flow reactor).

In the case of a CH_4/N_2 plasma, a DBD typically occurs in the so-called filamentary regime, consisting of a large number of independent micro-discharge filaments. In these micro-discharges a large fraction of the electron energy is used for excitation, dissociation and ionization of the molecules, and hence to initiate the chemical reactions. This is the reason why including these micro-discharges in the simulations is of prime importance for a realistic description of the reaction chemistry. Again, we cannot treat the spatial aspect of filament formation in our 0D model, but we can mimic the filamentary behavior by simulating a large number of micro-discharge pulses as a function of time. For more information about this procedure, we refer to our previous work [10,45].

For the experiments an applied frequency of 23.5 kHz is used and a residence of 2.2 s, as calculated from the gas flow rate and the length of the reactor. To mimic these conditions we simulated triangular micro-discharge pulses of 30 ns, with a repetition frequency of 0.47 kHz, assuming that each molecule passes through only one micro-discharge every 100 half

cycles (see detailed discussion in our previous work) [10]. Furthermore, the maximum power deposition per pulse is defined in such a way that the total specific energy input (SEI) corresponds to the experimental values (i.e., in the order of 6 J cm^{-3}; see below).

$$\text{SEI}\ (\text{J}\cdot\text{cm}^{-3}) = \frac{\text{Power}\ (\text{J}\cdot\text{s}^{-1})}{\text{Gas flow rate}(\text{cm}^{-3}\cdot\text{s}^{-1})}$$

Fig. 2 illustrates the calculated electron density (N_e) and electron temperature (T_e) for one pulse as a function of time. The calculated maximum E_0/N is in the order of 200 Td. This results in a maximum N_e of ~$5.5\cdot10^{13}$ cm^{-3} and a maximum T_e of ~3 eV during the pulse. At the start of the pulse, T_e reaches its maximum of ~3 eV, as the electrons are heated by the electric field, whereas upon pulse termination, T_e drops significantly. N_e on the other hand increases with time during the pulse and reaches its maximum of 5.5×10^{13} cm^{-3} at the end of the pulse, as shown in Fig. 2. This is logical, as the power leads to the electron heating and subsequently it gives rise to electron impact ionization, creating electrons during the pulse. However, the electron density decays very slowly upon termination of the pulse, indicating low recombination rates and/or the fact that electrons might still be created in the early afterglow by heavy particle reactions. For all investigated CH_4/N_2 mixtures the maximum T_e was around ~3 eV, while the maximum N_e was in the order of 10^{12}–10^{14}, which are typical conditions for a DBD [28,46].

4. Results

4.1. *Effect of N_2 as impurity on CH_4 conversion and H_2 yield*

As mentioned above, there are always impurities present in natural gas, of which N_2 is the most important one, and these can influence the plasma chemistry and thus the conversion of CH_4 as well as the product yields. Therefore, the influence of N_2 as impurity in the range of 1–50,000 ppm on a CH_4 plasma is computationally investigated in this section. In Fig. 3, the calculated conversion of CH_4 and the yield of H_2 are plotted versus the N_2 concentration, for a residence time of 2.2 s and a SEI of 6 J cm^{-3}. The results indicate that the conversion decreases slightly from 3.4% to 2.9% (equals −15%) upon increase of the N_2 impurity. This decreasing trend is the result of the decreasing electron density, as will be discussed more thoroughly in section 4.2.2. The H_2 yield shows the same decreasing trend from 2.1% to 1.8% (equals −17%) upon increase of the N_2 impurity. This is logical since the H_2 yield is related to the CH_4 conversion, which is the only source of H atoms. The most abundant N containing reaction product is hydrogen cyanide (HCN), however, its density is three orders of magnitude lower than the N_2 concentration. Thus, this indicates that N_2 does almost not chemically react in the plasma under study, and the N_2 impurities only have a small indirect (i.e., electron density) influence on the conversion of CH_4 and the yield of H_2 and do not result in a significant production of nitrogen containing species.

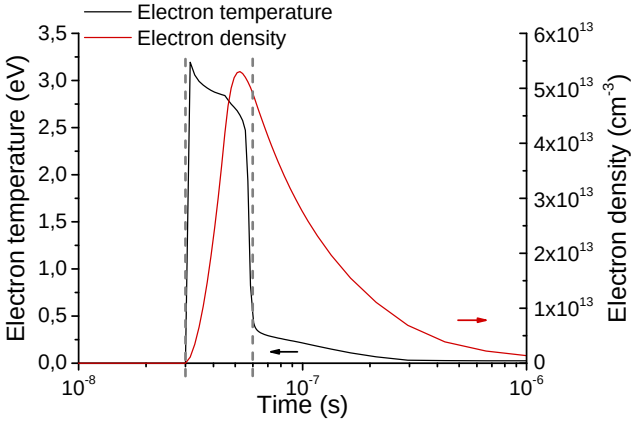

Fig. 2 – Calculated electron density (red line, right axis) and electron temperature (black line, left axis) during one triangular discharge pulse of 30 ns for a 95:5 CH_4/N_2 mixture. The grey dashed lines indicate the start and the end of the micro-discharge pulse. (For interpretation of the references to color in this figure legend, the reader is referred to the web version of this article.)

4.2. *Effect of N_2 as additive gas*

4.2.1. *Effect on CH_4 conversion and product yields*

Aside from studying the effect of N_2 as an impurity, it is also interesting to study the effect of N_2 as additive gas. The purpose is not only to study the effect on the conversion of CH_4 and the yield of H_2, but also to investigate whether nitrogenated compounds could be formed, which could be of interest as a feedstock for the chemical industry. Therefore, we performed both experiments and simulations for different mixtures of CH_4/N_2. We carried out experiments with a N_2 content of 1, 10, 19, 29, 39, 48, 58, 67, 77 and 87%. The same N_2 contents were also investigated in the simulations, as well as all (other) values in the range of 1–99% with a 2.5% interval. These simulations were performed for exactly the same operating conditions as in the experiments, i.e., a residence time of 2.2 s, a SEI of 6 J cm^{-3}, a gas temperature of 300 K and atmospheric pressure for all mixing ratios.

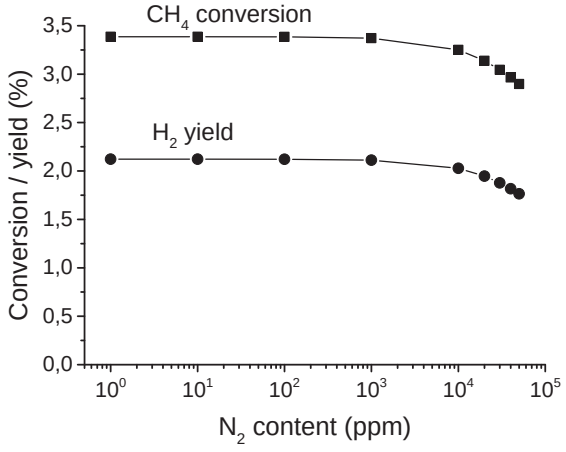

Fig. 3 – Calculated CH_4 conversion and H_2 yield as a function of N_2 content (ppm) for a residence time of 2.2 s and a SEI of 6 J cm^{-3}.

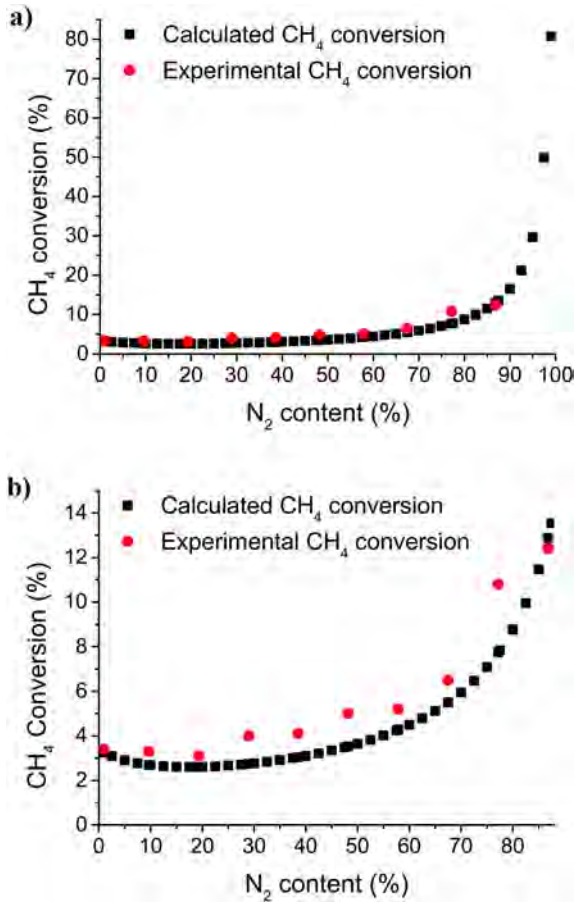

Fig. 4 – Calculated and experimental values of CH_4 conversion as a function of N_2 content in the entire range from 1 to 99% (a), and more detailed comparison from 1 to 88% (b), for a residence time of 2.2 s and a SEI of 6 J cm^{-3}.

The calculated and measured values for the conversion of CH_4 are plotted versus N_2 content in Fig. 4. Fig. 4(a) shows the results for the N_2 content in the entire range from 1 to 99%, while Fig. 4(b) presents the more detailed results for a N_2 content ranging only till 88%. It is clear that excellent agreement is reached between calculated and measured results.

From the simulation results in Fig. 4(a) it appears that the CH_4 conversion is increasing exponentially with increasing N_2 content, however, if we take a closer look to Fig. 4(b), we notice that for low N_2 content the conversion slightly decreases first, as was also observed in the ppm range (see previous section). Indeed, the calculated conversion decreases slightly from 3.4% to 2.6% for a N_2 content ranging from 0 to 17.5%. Subsequently, it starts increasing slightly, reaching 3.4% again for a N_2 content of 45%. It continues increasing and for a N_2 content above ~70% the increasing trend starts to become more significant. This trend is the result of the interplay of several effects, i.e. the decreasing electron density with increasing N_2 content, the lower reaction rate constants for several three-body reactions with N_2 compared to CH_4 as third body, and the increasing role of the N_2 metastable states with increasing N_2 content. These effects will be discussed more thoroughly in Section 4.2.2 and 4.2.3.

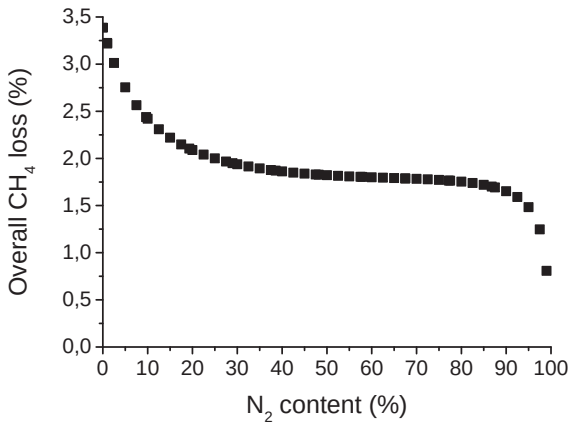

Fig. 5 – Calculated overall CH_4 loss as a function of N_2 content, for a residence time of 2.2 s and a SEI of 6 J cm^{-3}.

Although the absolute conversion increases with rising N_2 content, it does not compensate for the inherent drop of CH_4 content in the mixture, resulting in a lower overall CH_4 loss (in %), as shown in Fig. 5.

$$\text{Overall } CH_4\text{loss}(\%) = CH_4\text{content}(\%) \times CH_4\text{conversion}(\%)$$

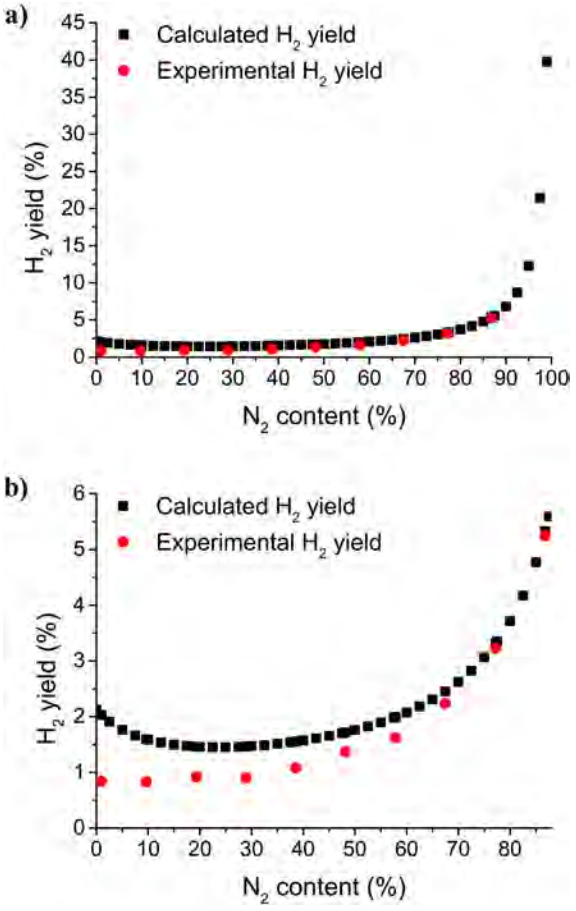

Fig. 6 – Calculated and experimental H_2 yield as a function of N_2 content in the entire range from 1 to 99% (a), and more detailed comparison from 1 to 88% (b), for a residence time of 2.2 s and a SEI of 6 J cm^{-3}.

It is clear that the CH_4 conversion obtained both in the experiments and calculations is in the order of several %, increasing only to 80% for very high N_2 contents. This reflects the high stability of the CH_4 molecule. Note that these values are in agreement with experimental results, at least for pure CH_4 conversion in a DBD [47–49].

The calculated and measured values for the H_2 yield are presented in Fig. 6. Again, Fig. 6(a) shows the results for a N_2 content ranging from 1 to 99%, while Fig. 6(b) presents the results in more detail for a N_2 content up to 88%. We only present the yields of H_2, since it is the most important reaction product. Its density is almost one order of magnitude higher than the second most import reaction product (i.e. C_2H_6); other hydrocarbons detected with the GC are C_2H_2, C_2H_4, C_3H_x and C_4H_y, but they have an even lower density. The H_2 selectivity is calculated to be around 40–60% for all CH_4/N_2 gas mixing ratios investigated. This means that for every mole CH_4 converted 1 mol H_2 is produced; the remaining H atoms are "lost" in the formation of higher hydrocarbons.

The H_2 yield is in the order of 1–2% up to 50% N_2 content, and increases to 40% at a N_2 content of 99%. These values are again in agreement with literature results, at least for pure CH_4 conversion in a DBD [47–49]. Moreover, the H_2 yield shows the same trend upon increasing N_2 content as the CH_4 conversion, as was also observed in the previous section, since CH_4 is the main source of H atoms. The somewhat lower experimental values for the H_2 yield are probably attributed to polymerization on the reactor walls, a phenomenon which is also observed in Horvath et al. [35]. Indeed a same polymerlike deposition (which is not accounted for in the simulations) was visible in our setup, resulting in a loss in the hydrogen and carbon balance after reaction. This can explain the difference between the calculated and experimental values. Furthermore, it should also be mentioned that determining the H_2 selectivity, and thus by extension the H_2 yield, with gas chromatography is quite challenging. However, overall, a satisfactory agreement between calculations and experiments is reached.

Again, the higher yield upon increasing N_2 content does not compensate for the inherent drop of CH_4 content in the mixture, resulting in a lower overall H_2 yield upon increasing N_2 content, as shown in Fig. 7.

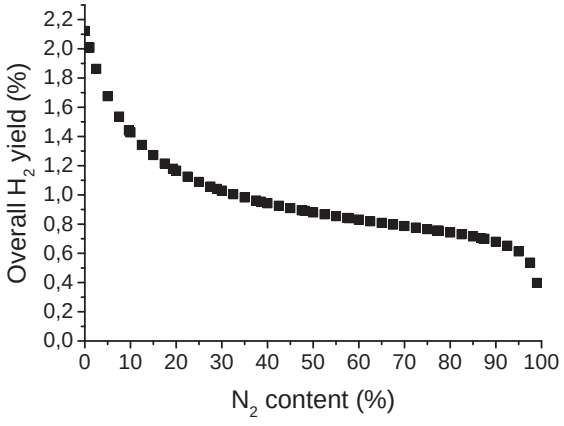

Fig. 7 – Calculated overall H_2 yield as a function of N_2 content, for a residence time of 2.2 s and a SEI of 6 J cm^{-3}.

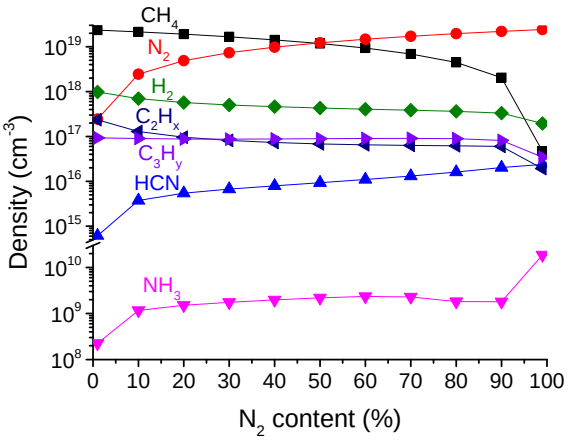

Fig. 8 – Calculated density of CH_4, N_2, H_2, C_2H_x, C_3H_y, HCN and NH_3 as a function of N_2 content (%) for a residence time of 2.2 s and a SEI of 6 J cm^{-3}.

Fig. 8 illustrates the calculated number densities of the main components present (or formed) in the plasma. CH_4, N_2 and H_2 have the highest density, as expected. The CH_4 density drops whereas the N_2 density rises with increasing N_2 content, as is logical. The H_2 density is around one order of magnitude lower than the CH_4 density, which is like expected from the conversion values (in the order of a few %) seen in Fig. 4 above. Only at high N_2 contents (i.e. above 90%), the H_2 density becomes larger than the CH_4 density, which corresponds to the high conversion, illustrated in Fig. 4 above. The densities of the higher hydrocarbon molecules (grouped as C_2H_x and C_3H_y) are at least an order of magnitude lower than the H_2 density.

As mentioned above, one of the reasons why we are interested in studying the effect of higher N_2 contents in the gas mixture is because of the possibility of forming N-containing products, which can be of interest for the chemical industry. The simulations indicate that some N-containing species are formed, such as HCN and NH_3, and that their densities increase with rising N_2 content, as shown in Fig. 8. However, their densities are always several orders of magnitude lower than the N_2 density. The most abundant N-containing species is HCN, which increases from $6\cdot10^{14}$ cm^{-3} (i.e., 25 ppm with respect to the density corresponding to atmospheric pressure) at 1% N_2, to $2.4\cdot10^{16}$ cm^{-3} (i.e., 1000 ppm) at 99% N_2 content. NH_3 is still of lower importance, with a density around 10^9 cm^{-3}, or a concentration in the order of only 0.1 ppb. This is in qualitative agreement with our experiments, since no N-containing species were detected. It should be mentioned that the production of HCN and NH_3 in CH_4/N_2 mixtures was reported for packed bed DBD and other discharges in literature [15–18,20,25], and it was mainly attributed to ionization of N_2 molecules. However, the latter process occurs at higher electron energy than is reached for our operating conditions, explaining why our calculations predict only negligible amounts of HCN and NH_3 formed.

As the calculated and experimental results for the CH_4 conversion and the H_2 yield are in good agreement in the

entire range of CH_4/N_2 gas mixing ratios (see Figs. 4 and 6), the plasma chemistry in the model can be used to describe and explain the observed trends, as will be done in the next two sections.

4.2.2. *Effect on the electron density*

To explain the effect of the N_2 content on the CH_4 conversion, we should first take a look at the effect of the N_2 content on the electron density. The maximum electron density for each CH_4/N_2 mixture is illustrated in Fig. 9.

The maximum electron density drops significantly upon increasing the N_2 content: it decreases almost exponentially from 4.1×10^{13} cm^{-3} at 1% N_2 content to 4.8×10^{12} cm^{-3} at 99% N_2 content. This is explained by the lower electron production rate, which is dependent on electron impact ionization reactions. The most important electron production reactions are:

$$e^- + CH_4 \rightarrow CH_4^+ + 2e^- \quad (1)$$

$$e^- + CH_4 \rightarrow CH_3^+ + H + 2e^- \quad (2)$$

$$e^- + N_2 \rightarrow N_2^+ + 2e^- \quad (3)$$

For a N_2 content up to ~ 88%, reactions 1 and 2 are the main contributors for electron production, whereas reaction 3 becomes the dominant electron production process for N_2 contents above 88%. As the ionization potential of N_2 (i.e., 15.6 eV for reaction 3) is higher than for CH_4 (i.e., 12.6 eV and 14.3 eV for reactions 1 and 2), the electron production by electron impact ionization of N_2 is less efficient than by electron impact ionization of CH_4, explaining the lower electron production rate upon increasing N_2 content.

4.2.3. *Kinetic analysis*

a) N_2 metastable states

As illustrated in Figs. 4 and 6, the CH_4 conversion and H_2 yield increase with increasing N_2 content, and this is attributed to collisions of CH_4 with singlet and triplet N_2 metastable states (i.e., $N_2(a'^1\sum_u^-)$ and $N_2(A^3\sum_u^+)$), as will be shown below.

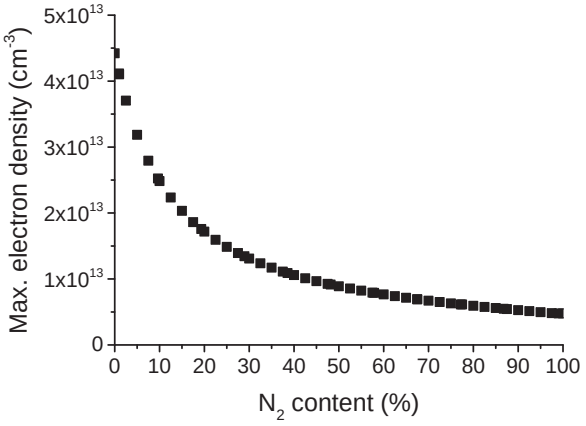

Fig. 9 – Calculated maximum electron density as a function of N_2 content (ranging from 1 to 99%) for a residence time of 2.2 s and a SEI of 6 J cm^{-3}.

Therefore, it is interesting to start our kinetic analysis with looking at the production and loss processes of these N_2 metastable states.

The densities of the two N_2 metastable states included in the model, i.e., the singlet $N_2(a'^1\sum_u^-)$ and triplet $N_2(A^3\sum_u^+)$ states, are plotted in Fig. 10, during one pulse and afterglow for a N_2 content of 50% and a SEI of 6 J cm^{-3}. It is clear that their densities, at the maximum of their profile, are several orders of magnitude lower than the N_2 ground state density, as shown in Fig. 8. The triplet $N_2(A^3\sum_u^+)$ state has the highest density (which is three orders of magnitude lower than the N_2 ground state density) and it occurs during the pulse and afterglow, while the singlet $N_2(a'^1\sum_u^-)$ state has a density which is still three orders of magnitude lower, and it only occurs during the pulse. These trends will be explained below based on the reaction rates.

The production of $N_2(a'^1\sum_u^-)$ and $N_2(A^3\sum_u^+)$ takes place during the discharge pulse and is caused by electron impact excitation:

$$e^- + N_2 \rightarrow e^- + N_2\left(a'^1\sum\nolimits_u^-\right) \quad (4)$$

$$e^- + N_2 \rightarrow e^- + N_2\left(A^3\sum\nolimits_u^+\right) \quad (5)$$

The production rate of these metastable states increases with increasing N_2 content, which is logical. Furthermore, the production rate of the triplet state is found to be one order of magnitude higher than for the singlet state, due to the lower excitation threshold, i.e. 6.17 eV for the triplet state compared to 8.4 eV for the singlet state [34].

For the singlet state, the most important loss channels are the Penning dissociation reactions with CH_4, which only take place during the pulse:

$$N_2\left(a'^1\sum\nolimits_u^-\right) + CH_4 \rightarrow CH_3 + H + N_2 \quad (6)$$

$$N_2\left(a'^1\sum\nolimits_u^-\right) + CH_4 \rightarrow C + 2H_2 + N_2 \quad (7)$$

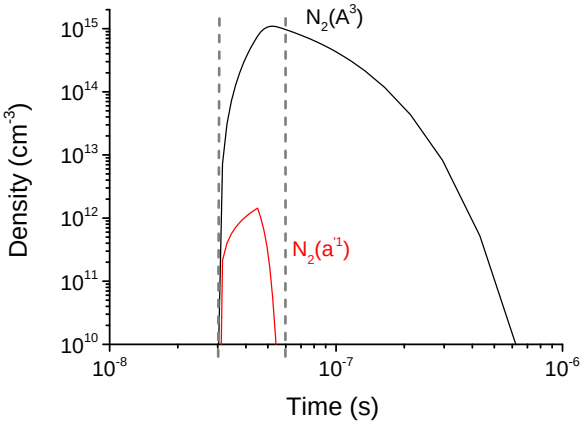

Fig. 10 – Calculated density of the $N_2(a'^1\sum_u^-)$ and $N_2(A^3\sum_u^+)$ states during one pulse and afterglow for a N_2 content of 50% and a SEI of 6 J cm^{-3}. The grey dashed lines indicate the start and the end of the micro-discharge pulse.

Table 2 – Overview of the most important loss and formation reactions for CH_4.

Loss processes		Formation processes	
L1	$e^- + CH_4 \rightarrow e^- + CH_3 + H$	F1	$CH_3 + H + CH_4 \rightarrow CH_4 + CH_4$
L2	$e^- + CH_4 \rightarrow e^- + CH_2 + H_2$	F2	$CH_3 + H + N_2 \rightarrow CH_4 + N_2$
L3	$N_2(A^3\sum_u^+) + CH_4 \rightarrow N_2 + CH_3 + H$	F3	$e^- + C_3H_8 \rightarrow CH_4 + C_2H_4 + e^-$
L4	$N_2(a'^1\sum_u^-) + CH_4 \rightarrow N_2 + CH_3 + H$	F4	$e^- + C_3H_6 \rightarrow CH_4 + C_2H_2 + e^-$
L5	$N_2(a'^1\sum_u^-) + CH_4 \rightarrow N_2 + C + 2H_2$		
L6	$CH + CH_4 \rightarrow C_2H_4 + H$		
L7	$C_2H + CH_4 \rightarrow C_2H_2 + CH_3$		

For the triplet state, the most important loss channel is the quenching reaction with H_2, followed by the Penning dissociation reaction with CH_4:

$$N_2\left(A^3\sum_u^+\right) + H_2 \rightarrow H_2 + N_2 \quad (8)$$

$$N_2\left(A^3\sum_u^+\right) + CH_4 \rightarrow CH_3 + H + N_2 \quad (9)$$

The quenching reaction takes place during the pulse as well as during the afterglow. For low N_2 contents, the quenching during the pulse appears to be dominant, but with increasing N_2 content, quenching in the afterglow becomes more important. Indeed, a higher N_2 content results in a higher density of the metastable triplet state, and a lower CH_4 and hence also lower H_2 density. As a result, not all the metastable states are quenched during the pulse, so the quenching continues in the afterglow and the latter becomes more and more important with increasing N_2 content.

Overall, the singlet state is found to be quenched more significantly than the triplet state, in agreement with literature [34]. The combination of higher production rate for the triplet state and higher quenching rate of the singlet state, explains why the triplet state has a higher density than the singlet state, as is indeed apparent from Fig. 10 above.

As the triplet state has a higher density than the singlet state, it will be the more important for the conversion of CH_4. On the other hand, the singlet state appears to be more important for the production of H_2, as will be shown below. This is explained because the triplet state is mainly quenched by H_2, and dissociation of CH_4 into CH_3 and H (i.e., Reaction 9 above), whereas the singlet state is also quenched by the decomposition of CH_4 into C and $2H_2$ molecules (i.e., Reaction 7 above). The reason that this decomposition can occur with the singlet state and not with the triplet state is the higher energy content of the former (as explained at the beginning of this section).

b) Conversion of CH_4

In order to better understand the influence of the N_2 content on the CH_4 conversion, we investigated the dominant reaction pathways for the loss and formation of CH_4 for several N_2 contents (i.e., 1, 10, 20, 30, 40, 50, 60, 70, 80, 90 and 99%). This kinetic analysis was performed by looking at the time integrated rates of the various processes during the pulse(s), the afterglow(s), as well as for the total time of 2.2 s, including many pulses and afterglows.

Table 2 lists the most important loss (L1–L7) and formation (F1–F4) processes for CH_4 and in Fig. 11 the time integrated rates, as well as the relative contributions of these processes are plotted as a function of N_2 content, for the total time of 2.2 s, as well as for the pulse(s) and the afterglow(s). It is clear from this figure that CH_4 is mainly decomposed during the pulse (see Fig. 11(a2)), whereas its formation occurs more in the afterglow (see Fig. 11(a1)). The same behavior was seen in our previous work about dry reforming [10]. Furthermore, it is also clear that the dominant reaction pathways change with increasing N_2 content.

If we take a look at the loss processes first, we see a clear shift in dominant loss processes when going from low to high N_2 content. At low N_2 contents, the direct decomposition of CH_4 by electron impact reactions (i.e., mainly reaction L1) is the dominant loss process. However, with increasing N_2 content the role of the N_2 metastable singlet and triplet states becomes more important and especially reaction L3 (so-called Penning dissociation by the triplet state) becomes the dominant loss process. Only at 99% N_2 content, reactions L4 and L5 (i.e., Penning dissociation by the singlet state) become the dominant loss processes.

If we take a look at the formation processes, it appears that the three-body recombination of CH_3 radicals with H atoms, with either CH_4 or N_2 molecules as third body (i.e., reactions F1 and F2), is the dominant formation process, but we can again notice a clear shift upon increasing N_2 content: up to a N_2 content of 90%, the three-body recombination with CH_4 as third body (i.e., reaction F1) is dominant, while above 90% the three-body recombination with N_2 (i.e., reaction F2) becomes most important. This is logical, since the amount of CH_4 in the mixture decreases and the amount of N_2 increases. The reason why the relative contributions of both processes do not change symmetric with N_2 content is because the recombination with CH_4 as third body is 3 times more efficient than with N_2 as third body [50].

From this analysis we can draw the following conclusions: with increasing N_2 content the electron density drops, especially in the lower N_2 content range (up to about 20%), leading to lower rates for the electron impact dissociation reactions of CH_4 (i.e., reaction L1). Since this reaction is the prime source of CH_3, this results in a lower CH_3 density, which in turn results in lower rates for the recombination reactions (i.e., reactions F1 and F2; note that this cannot be seen in the plots of the relative contributions, but it can be deduced from Fig. 11(a1)). So the lower loss rate is partially countered by lower formation rates, which explains why there is only a very small drop in CH_4 conversion (as shown in Fig. 4 between 1 and 20% N_2)

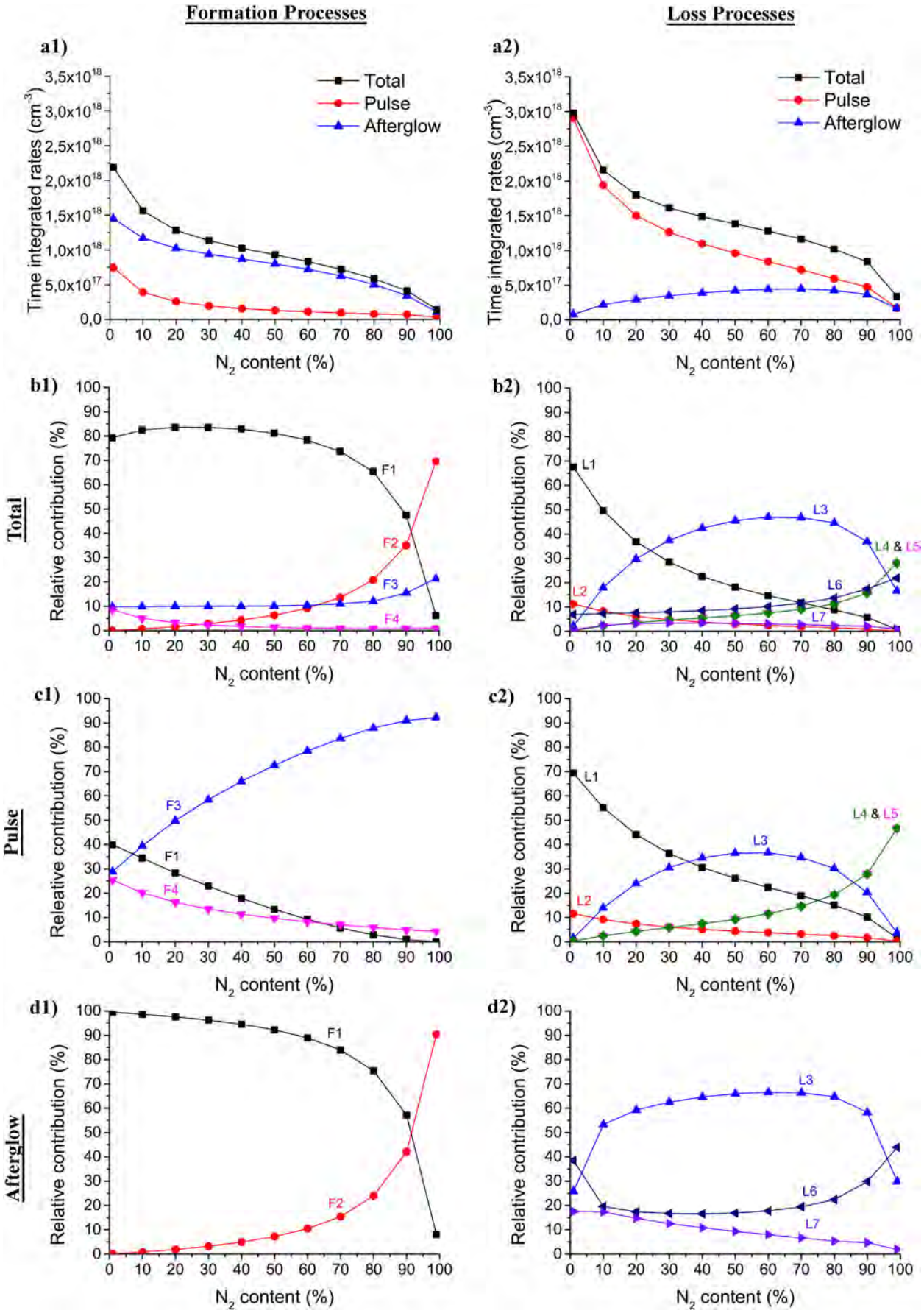

Fig. 11 – Time integrated rates of formation (a1) and loss (a2) of CH_4, and relative contributions of the various formation and loss processes for the total time (b1-2), the pulse(s) (c1-2) and the afterglow(s) (d1-2), as a function of N_2 content for a residence time of 2.2 s and a SEI of 6 J cm^{-3}. The numbers of the reactions correspond to the numbers of Table 2.

Table 3 – Overview of the most important loss and formation reactions for H_2.

Loss processes		Formation processes	
L1	$e^- + H_2 \rightarrow e^- + H + H$	F1	$e^- + CH_4 \rightarrow H_2 + CH_2 + e^-$
L2	$CH_2 + H_2 \rightarrow CH_3 + H$	F2	$e^- + CH_4 \rightarrow H_2 + H + CH + e^-$
L3	$C + H_2 \rightarrow CH + H$	F3	$e^- + C_3H_8 \rightarrow H_2 + C_3H_6 + e^-$
		F4	$e^- + C_2H_6 \rightarrow H_2 + C_2H_4 + e^-$
		F5	$CH_2 + CH_2 \rightarrow H_2 + C_2H_2$
		F6	$CH_2 + H \rightarrow H_2 + CH$
		F7	$N_2(a'^1\sum_u^-) + CH_4 \rightarrow 2H_2 + C + N_2$
		F8	$N_2(A^3\sum_u^+) + CH_4 \rightarrow H_2 + CH_2 + N_2$

compared to the significant drop in electron density. At the same time the role of the N_2 metastable states for the conversion of CH_4 increases (see L3–L5 in Fig. 11(b2)), explaining why the loss rate in Fig. 11(a2) drops less dramatically above 20% N_2 content, in spite of the fact that the electron density keeps decreasing (cf. Fig. 9 above). Furthermore, by comparing Fig. 11(a1) and (a2), it is clear that the total loss rate drops less than the total formation rate of CH_4 upon increasing N_2 content, so there will be a higher "absolute" conversion of CH_4. This explains why the CH_4 conversion starts increasing rapidly above 20% N_2 content, as seen in Fig. 4 above, due to dissociation upon collision with the N_2 metastable states.

c) Production of H_2

As H_2 is the prime product of the CH_4 conversion, with a selectivity of about 40–60% (see above), it is also of interest to take a look at the dominant reaction pathways for the formation and loss of H_2 for several N_2 contents (i.e., 1, 10, 20, 30, 40, 50, 60, 70, 80, 90 and 99%) to obtain a better understanding of the influence of the N_2 content on the H_2 yield. This kinetic analysis will be performed again by looking at the time integrated rates for the total time, the pulse(s) and the afterglow(s) of the simulations.

Table 3 lists the most important loss (L1–L3) and formation (F1–F8) processes for H_2 and Fig. 12 illustrates the time integrated rates as well as the relative contributions of these processes, for the above mentioned N_2 contents for the total time, the pulse(s) and the afterglow(s). From this figure it is clear that H_2 is almost exclusively formed during the pulse, whereas it can be decomposed both in the pulse and afterglow. However, when comparing Fig. 12(a1) and (a2), it is obvious that the formation rate is clearly higher than the loss rate, so there will be a net formation of H_2, for all N_2 contents, although it will drop slightly upon increasing N_2 content, in agreement with Fig. 7 above.

It also appears from Fig. 12 that the dominant reaction pathways again change drastically with increasing N_2 content. If we take a look at the production processes first, at low N_2 contents, the direct decomposition of CH_4 and higher hydrocarbons by electron impact reactions (i.e., reactions F1–F4) is the dominant formation process for H_2. However, with increasing N_2 content, the role of the N_2 metastable singlet state becomes increasingly important and reaction F7 becomes the dominant formation process for 30% N_2 content and above. As far as the loss processes are concerned, at very low N_2 content, electron impact dissociation of H_2 (i.e., reaction L1) is dominant, while with increasing N_2 content, reaction L3 rapidly becomes the most important loss process.

If we take a look at the relative contributions of formation and loss during pulse and afterglow (i.e., Fig. 12(c1-c2-d1-d2)), we see that even during the pulse the loss reaction L3 becomes more important as a loss process above 10% N_2 content, compared to electron impact dissociation (L1). During the afterglow, reaction L3 is dominant at all N_2 contents. Since the formation almost exclusively takes place during the pulse, Fig. 12(c1) looks exactly like Fig. 12(b1), except for the radical recombination reactions F5 and F6, which only occur during the afterglow, see Fig. 12(d1).

From these results it can be concluded that with increasing N_2 content the electron density drops, leading to lower rates for the electron impact dissociation reactions of CH_4 and higher hydrocarbons which produce H_2 (i.e., reaction F1–F4). At the same time, the rate of the dominant loss process L1, drops for the same reason. Furthermore, the rates of processes L2, F5 and F6 also drop because the prime source of CH_2 is electron impact dissociation of CH_4 (process F1). Quickly the role of the N_2 metastable singlet state increases (i.e., reaction F7), and becomes the dominant production process of H_2 above 30% N_2 content. Moreover, this reaction also leads to an increase in the production of C atoms, which was also observed experimentally by an increased amount of soot deposition in the plasma reactor. This higher C production in its turn leads to a higher rate of L3. Overall, the total H_2 formation rate is much higher than the total loss rate, so that there is a net formation of H_2 at all N_2 contents, although this overall formation drops upon increasing N_2 content, as was also shown in Fig. 7.

5. Conclusions

The goal of this paper was to investigate the effect of N_2 impurities (in the range of 1–50,000 ppm) as well as the effect of N_2 as additive gas (in the range of 1–99%) on the CH_4 conversion and on the H_2 yield, and to find out whether nitrogenated compounds could be formed. For this purpose a combined experimental and computational study was performed: a 0D chemical kinetics model, called "Global_kin" was applied to our experimental DBD setup.

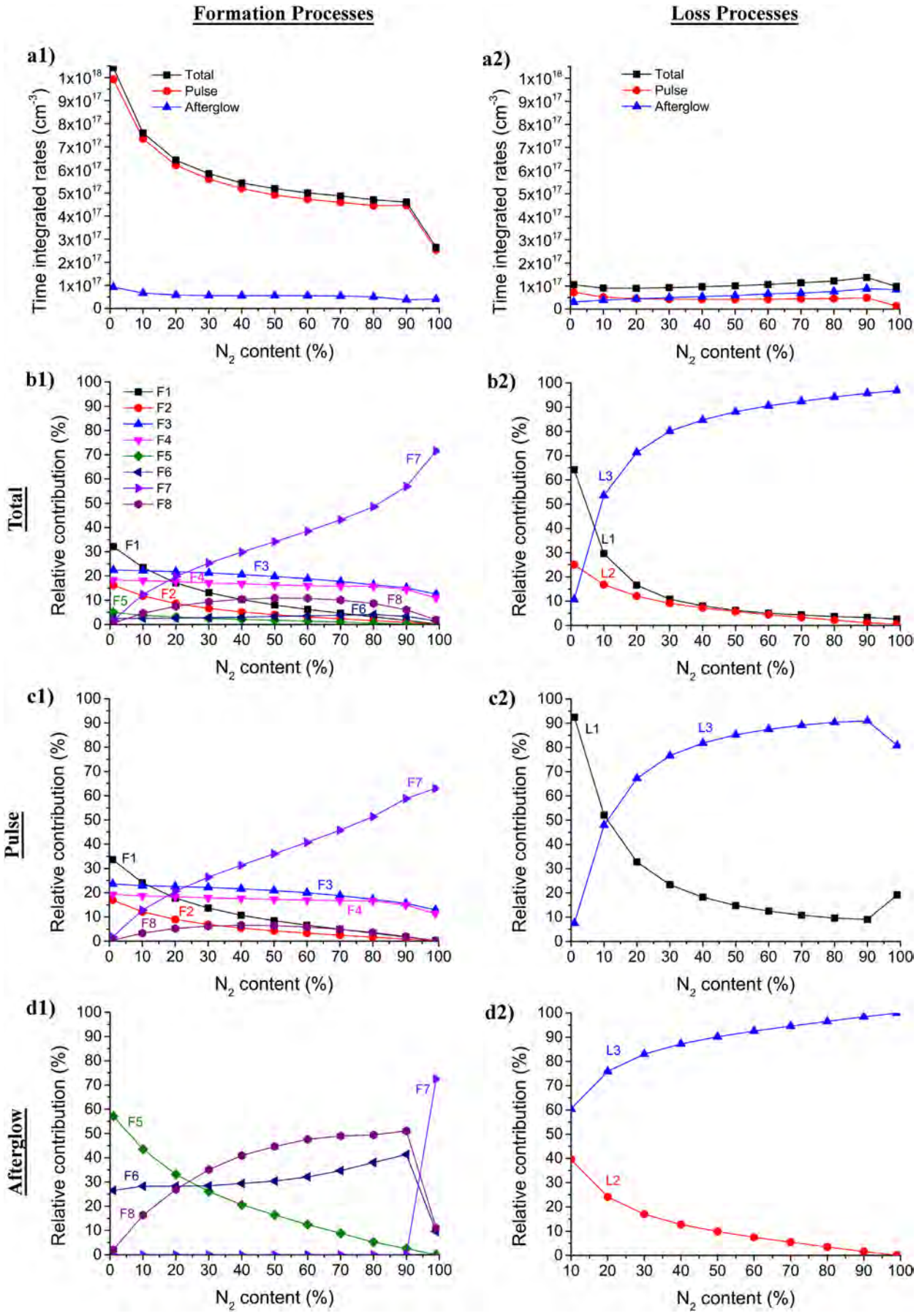

Fig. 12 – Time integrated rates of formation (a1) and loss (a2) of H_2, and relative contributions of the various formation and loss processes for the total time (b1-2), the pulse(s) (c1-2) and the afterglow(s) (d1-2), as a function of N_2 content for a residence time of 2.2 s and a SEI of 6 J cm^{-3}. The numbers of the reactions correspond to the numbers of Table 3.

The simulation results showed that the presence of N_2 impurities in the ppm range only has a minor indirect influence on the CH_4 conversion and H_2 yield, as a result of the decreasing electron density with increasing N_2 impurity content.

The experiments and simulations for the effect of N_2 as additive were in good agreement, for both CH_4 conversion and H_2 yield, in the entire range of CH_4/N_2 gas mixing ratios, allowing us to perform a kinetic analysis based on the modeling results.

The combined experimental and computational study revealed that increasing the N_2 content has a large influence on the CH_4 conversion and H_2 yield, since both clearly increase with N_2 content. These trends are the result of the interplay of several effects: (a) the decreasing electron density with increasing N_2 content lowers the contribution of the electron impact reactions for both the CH_4 loss and H_2 production; (b) the lower reaction rate constants for several three-body reactions with N_2 as third body compared to CH_4 lowers the recombination of species into CH_4, partly counteracting the lower CH_4 loss rates of the electron impact loss reactions; and (c) with increasing N_2 content the role of the N_2 metastable states becomes more important and Penning dissociation reactions with CH_4 become the dominant loss processes for CH_4 and the most important formation processes for H_2.

However, although the CH_4 conversion and H_2 yield increase upon rising N_2 content, this is not sufficient to counteract the inherent lower CH_4 content in the gas mixture with increasing N_2 content, thus the overall CH_4 conversion and overall H_2 yield drop upon increasing N_2 content. Finally, our calculations predict that only very low yields (in the ppm and ppb level) of nitrogenated compounds (i.e., HCN and NH_3) were produced, because the electron energy appears to be too low for efficient ionization of N_2, which was reported in literature to be the dominant precursor process for the formation of these nitrogenated compounds.

Acknowledgments

This work was supported by the IOF-SBO Project of the University of Antwerp, the Fund for Scientific Research Flanders (FWO), the Belgian Science Policy in the Framework of the Program Interuniversity Attraction Poles (IAP), and the Ministry of Science, Research and Technology of I. R. Iran. The authors would like to thank M. Kushner for providing the Globalkin code. Finally, this work was carried out in part using the Turing HPC infrastructure at CalcUA core facility of University of Antwerp, a division of the Flemish Supercomputer Center VSC, funded by the Hercules Foundation, the Flemish Government (department EWI) and the University of Antwerp.

Appendix A

Table A1 – Electron impact reactions with the various molecules and radicals, included in the model. These reactions are treated by energy-dependent cross sections, and the references where these cross sections were adopted from, are also included.

No.	Reaction	Rate coefficient	Ref.
1	$e^- + CH_4 \rightarrow C + H_2 + H_2 + e^-$	$f(\sigma)$	[10]
2	$e^- + CH_4 \rightarrow CH_4 + e^-$	$f(\sigma)$	[10]
3	$e^- + CH_4 \rightarrow CH_4^+ + e^- + e^-$	$f(\sigma)$	[10]
4	$e^- + CH_4 \rightarrow CH_3^+ + H + e^- + e^-$	$f(\sigma)$	[10]
5	$e^- + CH_4 \rightarrow CH_2^+ + H_2 + e^- + e^-$	$f(\sigma)$	[10]
6	$e^- + CH_4 \rightarrow CH_3 + H + e^-$	$f(\sigma)$	[10]
7	$e^- + CH_4 \rightarrow CH_2 + H_2 + e^-$	$f(\sigma)$	[10]
8	$e^- + CH_4 \rightarrow CH + H_2 + H + e^-$	$f(\sigma)$	[10]
9	$e^- + CH_3 \rightarrow CH_2^+ + H + e^- + e^-$	$f(\sigma)$	[10]
10	$e^- + CH_3 \rightarrow CH_2 + H + e^-$	$f(\sigma)$	[10]
11	$e^- + CH_3 \rightarrow CH + H_2 + e^-$	$f(\sigma)$	[10]
12	$e^- + CH_3 \rightarrow CH_3^+ + e^- + e^-$	$f(\sigma)$	[10]
13	$e^- + CH_3 \rightarrow CH^+ + H_2 + e^- + e^-$	$f(\sigma)$	[10]
14	$e^- + CH_2 \rightarrow CH^+ + H + e^- + e^-$	$f(\sigma)$	[10]
15	$e^- + CH_2 \rightarrow CH + H + e^-$	$f(\sigma)$	[10]
16	$e^- + CH_2 \rightarrow CH_2^+ + e^- + e^-$	$f(\sigma)$	[10]
17	$e^- + CH_2 \rightarrow C^+ + H_2 + e^- + e^-$	$f(\sigma)$	[10]
18	$e^- + CH \rightarrow C^+ + H + e^- + e^-$	$f(\sigma)$	[10]
19	$e^- + CH \rightarrow C + H + e^-$	$f(\sigma)$	[10]
20	$e^- + CH \rightarrow CH^+ + e^- + e^-$	$f(\sigma)$	[10]
21	$e^- + C \rightarrow C^+ + e^- + e^-$	$f(\sigma)$	[10]
22	$e^- + C_2H_6 \rightarrow C_2H_6 + e^-$	$f(\sigma)$	[10]
23	$e^- + C_2H_6 \rightarrow C_2H_6^+ + e^- + e^-$	$f(\sigma)$	[10]
24	$e^- + C_2H_6 \rightarrow C_2H_5^+ + H + e^- + e^-$	$f(\sigma)$	[10]
25	$e^- + C_2H_6 \rightarrow C_2H_4^+ + H_2 + e^- + e^-$	$f(\sigma)$	[10]
26	$e^- + C_2H_6 \rightarrow C_2H_3^+ + H_2 + H + e^- + e^-$	$f(\sigma)$	[10]

(continued on next page)

Table A1 – (*continued*)

No.	Reaction	Rate coefficient	Ref.
27	$e^- + C_2H_6 \rightarrow C_2H_2^+ + H_2 + H_2 + e^- + e^-$	$f(\sigma)$	[10]
28	$e^- + C_2H_6 \rightarrow CH_3^+ + CH_3 + e^- + e^-$	$f(\sigma)$	[10]
29	$e^- + C_2H_6 \rightarrow C_2H_5 + H + e^-$	$f(\sigma)$	[10]
30	$e^- + C_2H_6 \rightarrow C_2H_4 + H_2 + e^-$	$f(\sigma)$	[10]
31	$e^- + C_2H_5 \rightarrow C_2H_4^+ + H + e^- + e^-$	$f(\sigma)$	[10]
32	$e^- + C_2H_5 \rightarrow C_2H_3^+ + H_2 + e^- + e^-$	$f(\sigma)$	[10]
33	$e^- + C_2H_5 \rightarrow C_2H_2^+ + H_2 + H + e^- + e^-$	$f(\sigma)$	[10]
34	$e^- + C_2H_5 \rightarrow C_2H_4 + H + e^-$	$f(\sigma)$	[10]
35	$e^- + C_2H_5 \rightarrow C_2H_3 + H_2 + e^-$	$f(\sigma)$	[10]
36	$e^- + C_2H_5 \rightarrow C_2H_5^+ + e^- + e^-$	$f(\sigma)$	[10]
37	$e^- + C_2H_4 \rightarrow C_2H_4 + e^-$	$f(\sigma)$	[10]
38	$e^- + C_2H_4 \rightarrow C_2H_4^+ + e^- + e^-$	$f(\sigma)$	[10]
39	$e^- + C_2H_4 \rightarrow C_2H_3^+ + H + e^- + e^-$	$f(\sigma)$	[10]
40	$e^- + C_2H_4 \rightarrow C_2H_2^+ + H_2 + e^- + e^-$	$f(\sigma)$	[10]
41	$e^- + C_2H_4 \rightarrow C_2H_3 + H + e^-$	$f(\sigma)$	[10]
42	$e^- + C_2H_4 \rightarrow C_2H_2 + H_2 + e^-$	$f(\sigma)$	[10]
43	$e^- + C_2H_3 \rightarrow C_2H_2^+ + H + e^- + e^-$	$f(\sigma)$	[10]
44	$e^- + C_2H_3 \rightarrow C_2H^+ + H_2 + e^- + e^-$	$f(\sigma)$	[10]
45	$e^- + C_2H_3 \rightarrow C_2H_2 + H + e^-$	$f(\sigma)$	[10]
46	$e^- + C_2H_3 \rightarrow C_2H + H_2 + e^-$	$f(\sigma)$	[10]
47	$e^- + C_2H_3 \rightarrow C_2H_3^+ + e^- + e^-$	$f(\sigma)$	[10]
48	$e^- + C_2H_2 \rightarrow C_2H_2 + e^-$	$f(\sigma)$	[10]
49	$e^- + C_2H_2 \rightarrow C_2H_2^+ + e^- + e^-$	$f(\sigma)$	[10]
50	$e^- + C_2H_2 \rightarrow C_2H + H + e^-$	$f(\sigma)$	[10]
51	$e^- + C_2H_2 \rightarrow C_2 + H_2 + e^-$	$f(\sigma)$	[10]
52	$e^- + C_2H \rightarrow C_2H^+ + e^- + e^-$	$f(\sigma)$	[10]
53	$e^- + C_2H \rightarrow C_2 + H + e^-$	$f(\sigma)$	[10]
54	$e^- + C_2H \rightarrow C + CH + e^-$	$f(\sigma)$	[10]
55	$e^- + C_2 \rightarrow C_2^+ + e^- + e^-$	$f(\sigma)$	[10]
56	$e^- + C_2 \rightarrow C + C + e^-$	$f(\sigma)$	[10]
57	$e^- + C_3H_8 \rightarrow C_3H_8 + e^-$	$f(\sigma)$	[10]
58	$e^- + C_3H_8 \rightarrow C_2H_5^+ + CH_3 + e^- + e^-$	$f(\sigma)$	[10]
59	$e^- + C_3H_8 \rightarrow C_2H_4^+ + CH_4 + e^- + e^-$	$f(\sigma)$	[10]
60	$e^- + C_3H_8 \rightarrow C_3H_7 + H + e^-$	$f(\sigma)$	[10]
61	$e^- + C_3H_8 \rightarrow C_2H_4 + CH_4 + e^-$	$f(\sigma)$	[10]
62	$e^- + C_3H_8 \rightarrow C_3H_6 + H_2 + e^-$	$f(\sigma)$	[10]
63	$e^- + C_3H_7 \rightarrow C_2H_5^+ + CH_2 + e^- + e^-$	$f(\sigma)$	[10]
64	$e^- + C_3H_7 \rightarrow C_2H_4^+ + CH_3 + e^- + e^-$	$f(\sigma)$	[10]
65	$e^- + C_3H_7 \rightarrow C_2H_3^+ + CH_4 + e^- + e^-$	$f(\sigma)$	[10]
66	$e^- + C_3H_7 \rightarrow CH_3^+ + C_2H_4 + e^- + e^-$	$f(\sigma)$	[10]
67	$e^- + C_3H_7 \rightarrow C_2H_4 + CH_3 + e^-$	$f(\sigma)$	[10]
68	$e^- + C_3H_7 \rightarrow C_2H_3 + CH_4 + e^-$	$f(\sigma)$	[10]
69	$e^- + C_3H_7 \rightarrow C_3H_6 + H + e^-$	$f(\sigma)$	[10]
70	$e^- + C_3H_7 \rightarrow C_3H_5 + H_2 + e^-$	$f(\sigma)$	[10]
71	$e^- + C_3H_6 \rightarrow C_2H_5^+ + CH + e^- + e^-$	$f(\sigma)$	[10]
72	$e^- + C_3H_6 \rightarrow C_2H_4^+ + CH_2 + e^- + e^-$	$f(\sigma)$	[10]
73	$e^- + C_3H_6 \rightarrow C_2H_3^+ + CH_3 + e^- + e^-$	$f(\sigma)$	[10]
74	$e^- + C_3H_6 \rightarrow C_2H_2^+ + CH_4 + e^- + e^-$	$f(\sigma)$	[10]
75	$e^- + C_3H_6 \rightarrow CH_3^+ + C_2H_3 + e^- + e^-$	$f(\sigma)$	[10]
76	$e^- + C_3H_6 \rightarrow C_3H_5 + H + e^-$	$f(\sigma)$	[10]
77	$e^- + C_3H_6 \rightarrow C_2H_2 + CH_4 + e^-$	$f(\sigma)$	[10]
78	$e^- + C_3H_5 \rightarrow C_2H_3^+ + CH_2 + e^- + e^-$	$f(\sigma)$	[10]
79	$e^- + C_3H_5 \rightarrow C_2H_2^+ + CH_3 + e^- + e^-$	$f(\sigma)$	[10]
80	$e^- + C_3H_5 \rightarrow CH_3^+ + C_2H_2 + e^- + e^-$	$f(\sigma)$	[10]
81	$e^- + C_3H_5 \rightarrow C_2H_2 + CH_3 + e^-$	$f(\sigma)$	[10]
82	$e^- + H_2 \rightarrow e^- + H_2$	$f(\sigma)$	[43]
83	$e^- + H_2 \rightarrow H_2(\text{rot.}) + e^-$	$f(\sigma)$	[43]
84	$e^- + H_2 \rightarrow H_2(\text{rot.}) + e^-$	$f(\sigma)$	[43]
85	$e^- + H_2 \rightarrow H_2(\text{vib.}) + e^-$	$f(\sigma)$	[43]
86	$e^- + H_2 \rightarrow H_2(\text{vib.}) + e^-$	$f(\sigma)$	[43]
87	$e^- + H_2 \rightarrow H_2^* + e^-$	$f(\sigma)$	[43]
88	$e^- + H_2 \rightarrow H_2^* + e^-$	$f(\sigma)$	[43]
89	$e^- + H_2 \rightarrow e^- + H + H$	$f(\sigma)$	[43]
90	$e^- + H_2 \rightarrow e^- + e^- + H_2^+$	$f(\sigma)$	[43]

Table A1 – (*continued*)

No.	Reaction	Rate coefficient	Ref.
91	$e^- + H_2^* \rightarrow H_2^* + e^-$	$f(\sigma)$	[43]
92	$e^- + H_2^* \rightarrow H_2 + e^-$	$f(\sigma)$	[43]
93	$e^- + H_2^* \rightarrow H_2^+ + e^- + e^-$	$f(\sigma)$	[43]
94	$e^- + H \rightarrow e^- + H$	$f(\sigma)$	[43]
95	$e^- + H \rightarrow H^* + e^-$	$f(\sigma)$	[43]
96	$e^- + H \rightarrow H^* + e^-$	$f(\sigma)$	[43]
97	$e^- + H \rightarrow H^* + e^-$	$f(\sigma)$	[43]
98	$e^- + H \rightarrow e^- + H^+ + e^-$	$f(\sigma)$	[43]
99	$e^- + H^* \rightarrow H^* + e^-$	$f(\sigma)$	[43]
100	$e^- + H^* \rightarrow H + e^-$	$f(\sigma)$	[43]
101	$e^- + H^* \rightarrow H^+ + e^- + e^-$	$f(\sigma)$	[43]
102	$e^- + N_2 \rightarrow e^- + N_2$	$f(\sigma)$	[43]
103	$e^- + N_2 \rightarrow e^- + N_2(\text{rot.})$	$f(\sigma)$	[43]
104	$e^- + N_2 \rightarrow N_2(\text{vib.}) + e^-$	$f(\sigma)$	[43]
105	$e^- + N_2 \rightarrow N_2(\text{vib.}) + e^-$	$f(\sigma)$	[43]
106	$e^- + N_2 \rightarrow N_2(\text{vib.}) + e^-$	$f(\sigma)$	[43]
107	$e^- + N_2 \rightarrow N_2(\text{vib.}) + e^-$	$f(\sigma)$	[43]
108	$e^- + N_2 \rightarrow N_2(\text{vib.}) + e^-$	$f(\sigma)$	[43]
109	$e^- + N_2 \rightarrow N_2(\text{vib.}) + e^-$	$f(\sigma)$	[43]
110	$e^- + N_2 \rightarrow N_2(\text{vib.}) + e^-$	$f(\sigma)$	[43]
111	$e^- + N_2 \rightarrow e^- + N_2(A^3)$	$f(\sigma)$	[43]
112	$e^- + N_2 \rightarrow e^- + N_2(a'^1)$	$f(\sigma)$	[43]
113	$e^- + N_2 \rightarrow e^- + N + N$	$f(\sigma)$	[43]
114	$e^- + N_2 \rightarrow e^- + N^+ + N + e^-$	$f(\sigma)$	[43]
115	$e^- + N_2 \rightarrow e^- + e^- + N_2^+$	$f(\sigma)$	[43]
116	$e^- + N_2(\text{vib.}) \rightarrow N_2(\text{vib.}) + e^-$	$f(\sigma)$	[43]
117	$e^- + N_2(\text{vib.}) \rightarrow N_2 + e^-$	$f(\sigma)$	[43]
118	$e^- + N_2(\text{vib.}) \rightarrow N_2(A^3) + e^-$	$f(\sigma)$	[43]
119	$e^- + N_2(\text{vib.}) \rightarrow N_2^+ + e^- + e^-$	$f(\sigma)$	[43]
120	$e^- + N_2(A^3) \rightarrow e^- + N_2(A^3)$	$f(\sigma)$	[43]
121	$e^- + N_2(A^3) \rightarrow e^- + N_2$	$f(\sigma)$	[43]
122	$e^- + N_2(A^3) \rightarrow N_2(\text{vib.}) + e^-$	$f(\sigma)$	[43]
123	$e^- + N_2(A^3) \rightarrow e^- + N_2^+ + e^-$	$f(\sigma)$	[43]
124	$e^- + N_2(a'^1) \rightarrow N_2(a'^1) + e^-$	$f(\sigma)$	[43]
125	$e^- + N_2(a'^1) \rightarrow e^- + N_2$	$f(\sigma)$	[43]
126	$e^- + N_2(a'^1) \rightarrow N_2^+ + e^- + e^-$	$f(\sigma)$	[43]
127	$e^- + N \rightarrow e^- + N$	$f(\sigma)$	[43]
128	$e^- + N \rightarrow e^- + N^*$	$f(\sigma)$	[43]
129	$e^- + N \rightarrow e^- + N^+ + e^-$	$f(\sigma)$	[43]
130	$e^- + N^* \rightarrow e^- + N^*$	$f(\sigma)$	[43]
131	$e^- + N^* \rightarrow e^- + N$	$f(\sigma)$	[43]
132	$e^- + N^* \rightarrow e^- + N^+ + e^-$	$f(\sigma)$	[43]
133	$e^- + NH \rightarrow NH + e^-$	$f(\sigma)$	[43]
134	$e^- + NH \rightarrow N + H + e^-$	$f(\sigma)$	[43]
135	$e^- + NH \rightarrow N^+ + H + e^- + e^-$	$f(\sigma)$	[43]

Table A2 – Electron-ion reactions included in the model and the references where these data were adopted from. Some reactions are treated by energy-dependent cross sections, for others the reaction coefficients are given by the Arrhenius function: $k(T) = A\,(T/300\ \text{K})^n \exp(-E/RT)$ where T is the gas mixture temperature (in K) and A is given in units of $\text{cm}^3\ \text{s}^{-1}$ for two-body collisions and in $\text{cm}^6\ \text{s}^{-1}$ for three-body collisions. In the latter case, the values for A and n are listed in the table. If no values are listed for n and E/R, it means that these values are assumed to be zero, and the rate coefficient is just equal to A.

No.	Reaction	A	n	Ref
1	$e^- + CH_5^+ \rightarrow CH_3 + H + H$	2.57E-07	−0.30	[10]
2	$e^- + CH_5^+ \rightarrow CH_2 + H_2 + H$	6.61E-08	−0.30	[10]
3	$e^- + CH_4^+ \rightarrow CH_3 + H$	1.18E-08	−0.50	[10]
4	$e^- + CH_4^+ \rightarrow CH_2 + H + H$	2.42E-08	−0.50	[10]
5	$e^- + CH_4^+ \rightarrow CH + H_2 + H$	1.41E-08	−0.50	[10]
6	$e^- + CH_3^+ \rightarrow CH_2 + H$	2.25E-08	−0.50	[10]
7	$e^- + CH_3^+ \rightarrow CH + H_2$	7.88E-09	−0.50	[10]
8	$e^- + CH_3^+ \rightarrow CH + H + H$	9.00E-09	−0.50	[10]

(*continued on next page*)

Table A2 – (*continued*)

No.	Reaction	A	*n*	Ref
9	$e^- + CH_3^+ \rightarrow C + H_2 + H$	1.69E-08	−0.50	[10]
10	$e^- + CH_2^+ \rightarrow CH + H$	1.00E-08	−0.50	[10]
11	$e^- + CH_2^+ \rightarrow C + H_2$	4.82E-09	−0.50	[10]
12	$e^- + CH_2^+ \rightarrow C + H + H$	2.53E-08	−0.50	[10]
13	$e^- + CH^+ \rightarrow C + H$	3.23E-08	−0.42	[10]
14	$e^- + C_2H_6^+ \rightarrow C_2H_5 + H$	2.19E-08	−0.71	[10]
15	$e^- + C_2H_6^+ \rightarrow C_2H_4 + H + H$	3.36E-08	−0.71	[10]
16	$e^- + C_2H_5^+ \rightarrow C_2H_4 + H$	7.70E-09	−0.71	[10]
17	$e^- + C_2H_5^+ \rightarrow C_2H_3 + H + H$	1.92E-08	−0.71	[10]
18	$e^- + C_2H_5^+ \rightarrow C_2H_2 + H_2 + H$	1.60E-08	−0.71	[10]
19	$e^- + C_2H_5^+ \rightarrow C_2H_2 + H + H + H$	8.98E-09	−0.71	[10]
20	$e^- + C_2H_5^+ \rightarrow CH_3 + CH_2$	9.62E-09	−0.71	[10]
21	$e^- + C_2H_4^+ \rightarrow C_2H_3 + H$	8.29E-09	−0.71	[10]
22	$e^- + C_2H_4^+ \rightarrow C_2H_2 + H + H$	3.43E-08	−0.71	[10]
23	$e^- + C_2H_4^+ \rightarrow C_2H + H_2 + H$	5.53E-09	−0.71	[10]
24	$e^- + C_2H_3^+ \rightarrow C_2H_2 + H$	1.34E-08	−0.71	[10]
25	$e^- + C_2H_3^+ \rightarrow C_2H + H + H$	2.74E-08	−0.71	[10]
26	$e^- + C_2H_2^+ \rightarrow C_2H + H$	1.87E-08	−0.71	[10]
27	$e^- + C_2H_2^+ \rightarrow C_2 + H + H$	1.12E-08	−0.71	[10]
28	$e^- + C_2H_2^+ \rightarrow CH + CH$	4.87E-09	−0.71	[10]
29	$e^- + C_2H^+ \rightarrow C_2 + H$	1.34E-08	−0.71	[10]
30	$e^- + C_2H^+ \rightarrow CH + C$	1.09E-08	−0.71	[10]
31	$e^- + C_2H^+ \rightarrow C + C + H$	4.29E-09	−0.71	[10]
32	$e^- + C_2^+ \rightarrow C + C$	1.19E-08	−0.71	[10]
33	$e^- + H_3^+ \rightarrow H_2 + H$	$f(\sigma)$		[43]
34	$e^- + H_3^+ \rightarrow H + H + H$	$f(\sigma)$		[43]
35	$e^- + H_2^+ \rightarrow H + H$	$f(\sigma)$		[43]
36	$e^- + H^+ \rightarrow H$	$f(\sigma)$		[43]
37	$e^- + N_4^+ \rightarrow N_2 + N_2$	3.21E-07	−0.50	[43]
38	$e^- + N_4^+ \rightarrow N_2 + N + N$	3.13E-07	−0.41	[43]
39	$e^- + N_3^+ \rightarrow N + N_2$	3.22E-08	−0.50	[43]
40	$e^- + N_2^+ \rightarrow N + N$	$f(\sigma)$		[43]
41	$e^- + M + N_2^+ \rightarrow N_2 + M$	4.31E-34	−4.50	[43]
42	$e^- + N^+ \rightarrow N$	$f(\sigma)$		[43]
43	$e^- + N^+ + M \rightarrow N + M$	2.49E-29	−1.50	[43]
44	$e^- + H_3^+ \rightarrow H_3^+ + e^-$	$f(\sigma)$		[43]
45	$e^- + H_3^+ \rightarrow e^- + H_2 + H^+$	$f(\sigma)$		[43]
46	$e^- + H_3^+ \rightarrow e^- + H + H + H^+$	$f(\sigma)$		[43]
47	$e^- + H_2^+ \rightarrow e^- + H_2^+$	$f(\sigma)$		[43]
48	$e^- + H_2^+ \rightarrow e^- + H^+ + H$	$f(\sigma)$		[43]
49	$e^- + H_2^+ \rightarrow H^+ + H^-$	$f(\sigma)$		[43]
50	$e^- + H^+ \rightarrow e^- + H^+$	$f(\sigma)$		[43]
51	$e^- + H^+ + e^- \rightarrow e^- + H$	8.80E-27	−4.50	[43]
52	$e^- + H^- \rightarrow e^- + e^- + H$	$f(\sigma)$		[43]
53	$e^- + H^- \rightarrow e^- + H^-$	$f(\sigma)$		[43]
54	$e^- + N_4^+ \rightarrow e^- + N_4^+$	$f(\sigma)$		[43]
55	$e^- + N_3^+ \rightarrow e^- + N_3^+$	$f(\sigma)$		[43]
56	$e^- + N_2^+ \rightarrow e^- + N_2^+$	$f(\sigma)$		[43]
57	$e^- + e^- + N_2^+ \rightarrow N_2 + e^-$	7.18E-27	−4.50	[43]
58	$e^- + N^+ \rightarrow e^- + N^+$	$f(\sigma)$		[43]
59	$e^- + N^+ + e^- \rightarrow N + e^-$	5.40E-24	−4.50	[43]

Table A3 – Ion–ion reactions included in the model and the references where these data were adopted from. Reaction coefficients are given by the Arrhenius function: $k(T) = A\,(T/300\ K)^n \exp(-E/RT)$ where *T* is the gas mixture temperature (in K) and *A* is given in units of $cm^3\ s^{-1}$ for two-body collisions and in $cm^6\ s^{-1}$ for three-body collisions. If no values are listed for *n* and E/R, it means that these values are assumed to be zero, and the rate coefficient is just equal to *A*.

No.	Reaction	A	*n*	Ref.
1	$H^- + H_3^+ \rightarrow H_2 + H + H$	1.00E-07		[43]
2	$H^- + H_2^+ \rightarrow H + H_2$	2.00E-07	−0.50	[43]
3	$H^- + H_2^+ \rightarrow H + H + H$	1.00E-07		[43]
4	$H^- + H_2^+ + M \rightarrow H + H_2 + M$	2.00E-25	−2.50	[43]

Table A3 – (*continued*)

No.	Reaction	A	n	Ref.
5	$H^+ + H^- \rightarrow H + H$	2.00E-07	−0.50	[43]
6	$H^+ + H^- + M \rightarrow H + H + M$	2.00E-25	−2.50	[43]
7	$H^- + N_4^+ \rightarrow N_2 + N_2 + H$	1.00E-07		[43]
8	$H^- + N_3^+ \rightarrow NH + N_2$	3.00E-06	−0.50	[42]
9	$H^- + N_3^+ \rightarrow N + N_2 + H$	1.00E-07		[43]
10	$H^- + N_2^+ \rightarrow N_2 + H$	2.00E-07	−0.50	[43]
11	$H^- + N_2^+ \rightarrow N + N + H$	1.00E-07		[43]
12	$H^- + N_2^+ + M \rightarrow N_2 + H + M$	2.00E-25	−2.50	[43]
13	$H^- + N^+ \rightarrow N + H$	2.00E-07	−0.50	[43]
14	$H^- + N^+ + M \rightarrow NH + M$	2.00E-25	−2.50	[43]

Table A4 – Neutral–neutral reactions included in the model and the references where these data were adopted from. Reaction coefficients are given by the Arrhenius function: $k(T) = A\,(T/300\ K)^n \exp(-E/RT)$ where *T* is the gas mixture temperature (in K) and *A* is given in units of $cm^3\ s^{-1}$ for two-body collisions and in $cm^6\ s^{-1}$ for three-body collisions. If no values are listed for *n* and E/R, it means that these values are assumed to be zero, and the rate coefficient is just equal to *A*.

No.	Reaction	A	n	E/R	Ref.
1	$CH_4 + CH_2 \rightarrow CH_3 + CH_3$	3.01E-19			[10]
2	$CH_4 + CH \rightarrow C_2H_4 + H$	9.74E-11			[10]
3	$CH_4 + C_2H_5 \rightarrow C_2H_6 + CH_3$	1.83E-24			[10]
4	$CH_4 + C_2H_3 \rightarrow C_2H_4 + CH_3$	2.28E-18			[10]
5	$CH_4 + C_2H \rightarrow C_2H_2 + CH_3$	1.31E-12			[10]
6	$CH_4 + C_3H_7 \rightarrow C_3H_8 + CH_3$	4.38E-24			[10]
7	$CH_4 + H \rightarrow CH_3 + H_2$	8.43E-19			[10]
8	$CH_3 + CH_3 \rightarrow C_2H_5 + H$	2.71E-19			[10]
9	$CH_3 + CH_3 + CH_4 \rightarrow C_2H_6 + CH_4$	4.23E-29	−0.784	310	[33,50]
10	$CH_3 + CH_3 + N_2 \rightarrow C_2H_6 + N_2$	1.41E-29	−0.784	310	[33]
11	$CH_3 + CH_2 \rightarrow C_2H_4 + H$	7.01E-11			[10]
12	$CH_3 + C_2H_6 \rightarrow C_2H_5 + CH_4$	7.21E-21			[10]
13	$CH_3 + C_2H_5 \rightarrow C_2H_4 + CH_4$	1.91E-12			[10]
14	$CH_3 + C_2H_5 + CH_4 \rightarrow C_3H_8 + CH_4$	1.00E-28			[10]
15	$CH_3 + C_2H_5 + N_2 \rightarrow C_3H_8 + N_2$	1.00E-28			[10]
16	$CH_3 + C_2H_4 \rightarrow C_2H_3 + CH_4$	1.94E-21			[10]
17	$CH_3 + C_2H_3 \rightarrow C_2H_2 + CH_4$	6.51E-13			[10]
18	$CH_3 + C_2H_3 + CH_4 \rightarrow C_3H_6 + CH_4$	4.91E-30			[10]
19	$CH_3 + C_2H_3 + N_2 \rightarrow C_3H_6 + N_2$	4.91E-30			[10]
20	$CH_3 + C_2H_2 \rightarrow CH_4 + C_2H$	7.65E-26			[10]
21	$CH_3 + C_3H_8 \rightarrow C_3H_7 + CH_4$	1.02E-20			[10]
22	$CH_3 + C_3H_7 \rightarrow C_3H_6 + CH_4$	3.07E-12			[10]
23	$CH_3 + C_3H_6 \rightarrow C_3H_5 + CH_4$	1.24E-19			[10]
24	$CH_3 + H_2 \rightarrow CH_4 + H$	9.60E-21			[10]
25	$CH_3 + H \rightarrow CH_2 + H_2$	9.96E-22			[10]
26	$CH_3 + H + CH_4 \rightarrow CH_4 + CH_4$	2.97E-28			[10]
27	$CH_3 + H + N_2 \rightarrow CH_4 + N_2$	4.09E-29	−1.15	175	[33]
28	$CH_2 + CH_2 \rightarrow C_2H_2 + H_2$	5.27E-11			[10]
29	$CH_2 + C_2H_5 \rightarrow C_2H_4 + CH_3$	3.01E-11			[10]
30	$CH_2 + C_2H_3 \rightarrow C_2H_2 + CH_3$	3.01E-11			[10]
31	$CH_2 + C_2H \rightarrow C_2H_2 + CH$	3.01E-11			[10]
32	$CH_2 + C_3H_8 \rightarrow C_3H_7 + CH_3$	1.02E-20			[10]
33	$CH_2 + C_3H_7 \rightarrow C_2H_4 + C_2H_5$	3.01E-11			[10]
34	$CH_2 + C_3H_7 \rightarrow C_3H_6 + CH_3$	3.01E-12			[10]
35	$CH_2 + C_3H_6 \rightarrow C_3H_5 + CH_3$	3.65E-17			[10]
36	$CH_2 + H_2 \rightarrow CH_3 + H$	5.00E-15			[10]
37	$CH_2 + H \rightarrow CH + H_2$	2.01E-10			[10]
38	$CH + C_2H_6 + CH_4 \rightarrow C_3H_7 + CH_4$	1.14E-29			[10]
39	$CH + C_2H_6 + N_2 \rightarrow C_3H_7 + N_2$	1.14E-29			[10]
40	$CH + H_2 \rightarrow CH_2 + H$	6.80E-13			[10]
41	$CH + H \rightarrow C + H_2$	1.00E-10			[10]
42	$C + H_2 \rightarrow CH + H$	1.50E-10			[10]
43	$C_2H_6 + C_2H_3 \rightarrow C_2H_5 + C_2H_4$	3.39E-21			[10]
44	$C_2H_6 + C_2H \rightarrow C_2H_2 + C_2H_5$	5.99E-12			[10]

(*continued on next page*)

Table A4 – (*continued*)

No.	Reaction	A	*n*	E/R	Ref.
45	$C_2H_6 + C_3H_7 \rightarrow C_3H_8 + C_2H_5$	3.16E-22			[10]
46	$C_2H_6 + H \rightarrow C_2H_5 + H_2$	4.96E-17			[10]
47	$C_2H_5 + C_2H_5 \rightarrow C_2H_6 + C_2H_4$	2.41E-12			[10]
48	$C_2H_5 + C_2H \rightarrow C_2H_4 + C_2H_2$	3.01E-12			[10]
49	$C_2H_5 + C_3H_8 \rightarrow C_2H_6 + C_3H_7$	3.62E-22			[10]
50	$C_2H_5 + C_3H_7 \rightarrow C_3H_8 + C_2H_4$	1.91E-12			[10]
51	$C_2H_5 + C_3H_7 \rightarrow C_3H_6 + C_2H_6$	2.41E-12			[10]
52	$C_2H_5 + C_3H_6 \rightarrow C_3H_5 + C_2H_6$	2.53E-20			[10]
53	$C_2H_5 + C_3H_5 \rightarrow C_3H_6 + C_2H_4$	5.36E-12			[10]
54	$C_2H_5 + H_2 \rightarrow C_2H_6 + H$	2.97E-21			[10]
55	$C_2H_5 + H \rightarrow CH_3 + CH_3$	5.99E-11			[10]
56	$C_2H_5 + H \rightarrow C_2H_4 + H_2$	3.01E-12			[10]
57	$C_2H_5 + H + CH_4 \rightarrow C_2H_6 + CH_4$	9.20E-30			[10]
58	$C_2H_5 + H + N_2 \rightarrow C_2H_6 + N_2$	9.20E-30			[10]
59	$C_2H_4 + C_2H \rightarrow C_2H_2 + C_2H_3$	1.40E-10			[10]
60	$C_2H_4 + H \rightarrow C_2H_3 + H_2$	4.92E-21			[10]
61	$C_2H_4 + H + CH_4 \rightarrow C_2H_5 + CH_4$	3.66E-30			[10]
62	$C_2H_4 + H + N_2 \rightarrow C_2H_5 + N_2$	8.19E-30			[10]
63	$C_2H_3 + C_2H_3 \rightarrow C_2H_4 + C_2H_2$	1.60E-12			[10]
64	$C_2H_3 + C_2H \rightarrow C_2H_2 + C_2H_2$	1.60E-12			[10]
65	$C_2H_3 + C_3H_8 \rightarrow C_2H_4 + C_3H_7$	3.40E-21			[10]
66	$C_2H_3 + C_3H_7 \rightarrow C_3H_8 + C_2H_2$	2.01E-12			[10]
67	$C_2H_3 + C_3H_7 \rightarrow C_3H_6 + C_2H_4$	2.01E-12			[10]
68	$C_2H_3 + C_3H_6 \rightarrow C_3H_5 + C_2H_4$	6.58E-19			[10]
69	$C_2H_3 + C_3H_5 \rightarrow C_3H_6 + C_2H_2$	8.00E-12			[10]
70	$C_2H_3 + H_2 \rightarrow C_2H_4 + H$	9.78E-20			[10]
71	$C_2H_3 + H \rightarrow C_2H_2 + H_2$	2.01E-11			[10]
72	$C_2H_3 + H + CH_4 \rightarrow C_2H_4 + CH_4$	8.26E-30			[10]
73	$C_2H_3 + H + N_2 \rightarrow C_2H_4 + N_2$	8.26E-30			[10]
74	$C_2H_2 + C_2H \rightarrow C_4H_2 + H$	1.50E-10			[10]
75	$C_2H_2 + H \rightarrow C_2H + H_2$	6.12E-27			[10]
76	$C_2H_2 + H + CH_4 \rightarrow C_2H_3 + CH_4$	2.81E-31			[10]
77	$C_2H_2 + H + N_2 \rightarrow C_2H_3 + N_2$	5.05E-31			[10]
78	$C_2H + C_2H \rightarrow C_2H_2 + C_2$	3.01E-12			[10]
79	$C_2H + C_3H_8 \rightarrow C_2H_2 + C_3H_7$	5.99E-12			[10]
80	$C_2H + C_3H_7 \rightarrow C_3H_6 + C_2H_2$	1.00E-11			[10]
81	$C_2H + C_3H_6 \rightarrow C_3H_5 + C_2H_2$	5.99E-12			[10]
82	$C_2H + H_2 \rightarrow C_2H_2 + H$	1.52E-13			[10]
83	$C_2H + H + CH_4 \rightarrow C_2H_2 + CH_4$	9.44E-30			[10]
84	$C_2H + H + N_2 \rightarrow C_2H_2 + N_2$	9.44E-30			[10]
85	$C_3H_8 + H \rightarrow C_3H_7 + H_2$	5.15E-17			[10]
86	$C_3H_7 + C_3H_7 \rightarrow C_3H_6 + C_3H_8$	2.81E-12			[10]
87	$C_3H_7 + C_3H_6 \rightarrow C_3H_5 + C_3H_8$	2.53E-20			[10]
88	$C_3H_7 + C_3H_5 \rightarrow C_3H_6 + C_3H_6$	3.00E-12			[10]
89	$C_3H_7 + H_2 \rightarrow C_3H_8 + H$	7.12E-21			[10]
90	$C_3H_7 + H \rightarrow C_3H_6 + H_2$	3.01E-12			[10]
91	$C_3H_7 + H + CH_4 \rightarrow C_3H_8 + CH_4$	3.96E-30			[10]
92	$C_3H_7 + H + N_2 \rightarrow C_3H_8 + N_2$	3.96E-30			[10]
93	$C_3H_6 + H \rightarrow C_3H_5 + H_2$	6.94E-15			[10]
94	$C_3H_6 + H + CH_4 \rightarrow C_3H_7 + CH_4$	3.79E-33			[10]
95	$C_3H_6 + H + N_2 \rightarrow C_3H_7 + N_2$	3.79E-33			[10]
96	$C_3H_5 + H + CH_4 \rightarrow C_3H_6 + CH_4$	1.33E-29			[10]
97	$C_3H_5 + H + N_2 \rightarrow C_3H_6 + N_2$	1.33E-29			[10]
98	$CH_4 + CN \rightarrow CH_3 + HCN$	1.00E-11		857	[38]
99	$CH_4 + N + H \rightarrow NH + CH_4$	5.00E-32			[44]
100	$CH_3 + N \rightarrow HCN + H_2$	1.40E-11			[38]
101	$CH_3 + N \rightarrow H_2CN + H$	9.61E-11			[38]
102	$CH_2 + N \rightarrow HCN + H$	5.00E-11		250	[38]
103	$CH_2 + N \rightarrow CN + H + H$	1.60E-11			[38]
104	$CH_2 + N \rightarrow H_2 + CN$	1.60E-11			[33]
105	$C + N_2 \rightarrow CN + N$	1.04E-10		23,000	[38]
106	$C_2H_4 + N \rightarrow HCN + CH_3$	3.30E-14		353	[33]
107	$C_2H_2 + N \rightarrow CH + HCN$	2.70E-15			[33]
108	$C_3H_6 + N \rightarrow HCN + C_2H_5$	1.94E-13		654	[33]
109	$H_2 + H \rightarrow H + H + H$	4.67E-07	−1.00	55,000	[43]

Table A4 – (*continued*)

No.	Reaction	A	*n*	E/R	Ref.
110	$H_2 + N \rightarrow NH + H$	1.69E-09		18,095	[43]
111	$H_2 + N + NH_3 \rightarrow NH_2 + NH_3$	1.00E-36			[44]
112	$H_2 + CN \rightarrow H + HCN$	4.98E-19	2.45	1118	[38]
113	$H + HCN + N_2 \rightarrow H_2CN + N_2$	4.84E-30		2440	[33]
114	$H + H + CH_4 \rightarrow H_2 + CH_4$	6.00E-33			[10]
115	$H + H + H_2 \rightarrow H_2 + H_2$	4.00E-32	−1.00		[43]
116	$H + H + N_2 \rightarrow H_2 + N_2$	2.00E-32	−1.00		[43]
117	$H + N + N_2 \rightarrow NH + N_2$	5.00E-32			[43]
118	$H + N + H_2 \rightarrow NH + H_2$	1.00E-31			[43]
119	$H + NH_2 \rightarrow NH + H_2$	1.00E-11			[33]
120	$H + NH_2 + M \rightarrow NH_3 + M$	6.00E-30			[44]
121	$H + NH \rightarrow H_2 + N$	1.70E-11			[43]
122	$H + H_2CN \rightarrow HCN + H_2$	5.02E-10	0.50		[33]
123	$N_2 + CN \rightarrow N_2 + C + N$	4.15E-10		70,538.50	[38]
124	$N + CH \rightarrow CN + H$	2.10E-11			[33]
125	$N + CN \rightarrow C + N_2$	6.64E-11			[38]
126	$N + H_2CN \rightarrow HCN + NH$	6.70E-11			[38]
127	$N + N + N_2 \rightarrow N_2 + N_2$	1.38E-34		−500	[43]
128	$N + N + H_2 \rightarrow N_2 + H_2$	2.50E-34		−500	[43]
129	$N_2H_4 + N \rightarrow N_2H_2 + NH_2$	1.30E-13			[44]
130	$N_2H_4 + H \rightarrow N_2H_3 + H_2$	1.20E-11		1260	[44]
131	$N_2H_3 + H \rightarrow NH_2 + NH_2$	2.70E-12			[44]
132	$N_2H_4 + NH_2 \rightarrow NH_3 + N_2H_3$	5.20E-13			[44]
133	$N_2H_3 + N_2H_3 \rightarrow NH_3 + NH_3 + N_2$	5.00E-12			[44]
134	$N_2H_3 + N_2H_3 \rightarrow N_2H_4 + N_2H_2$	2.00E-11			[44]
135	$N_2H_2 + H \rightarrow N_2 + H_2 + H$	4.50E-13	2.63	−115	[44]
136	$N_2H_2 + NH_2 \rightarrow N_2 + H + NH_3$	1.50E-13	4.05	−810	[44]
137	$NH_3 + H \rightarrow H_2 + NH_2$	6.50E-13	2.76	5135	[44]
138	$NH_3 + NH + NH_3 \rightarrow N_2H_4 + NH_3$	1.00E-33			[44]
139	$NH_2 + H_2 \rightarrow NH_3 + H$	2.10E-12		4277	[44]
140	$NH_2 + N \rightarrow N_2 + H + H$	1.20E-10			[44]
141	$NH_2 + NH_2 + NH_3 \rightarrow N_2H_4 + NH_3$	6.90E-30			[44]
142	$NH_2 + NH_2 \rightarrow H_2 + N_2H_2$	6.60E-11		6000	[33]
143	$NH_2 + NH_2 \rightarrow NH + NH_3$	8.30E-11		5030	[33]
144	$NH_2 + NH_2 \rightarrow N_2H_4$	8.00E-11			[33]
145	$NH_2 + NH \rightarrow N_2H_3$	1.20E-10			[44]
146	$NH + N \rightarrow H + N_2$	2.50E-11			[43]
147	$NH + NH_2 \rightarrow H + N_2H_2$	5.25E-11		500	[33]
148	$NH + NH \rightarrow N_2H_2$	3.50E-12			[44]
149	$NH + NH + M \rightarrow H_2 + N_2 + M$	1.00E-33			[38]
150	$NH + NH \rightarrow H + N_2H$	2.29E-11	0.50	500	[33]
151	$NH + NH \rightarrow NH_2 + N$	5.72E-12	0.50	1000	[33]
152	$NH + NH \rightarrow N_2 + H + H$	1.20E-09			[43]
153	$NH + NH \rightarrow N_2 + H_2$	1.70E-11			[43]

Table A5 – Ion–neutral reactions included in the model and the references where these data were adopted from. Reaction coefficients are given by the Arrhenius function: $k(T) = A\,(T/300\ K)^n \exp(-E/RT)$ where *T* is the gas mixture temperature (in K) and *A* is given in units of $cm^3\ s^{-1}$ for two-body collisions and in $cm^6\ s^{-1}$ for three-body collisions.

No.	Reaction	A	*n*	E/R	Ref.
1	$CH_5^+ + CH_2 \rightarrow CH_3^+ + CH_4$	9.60E-10			[10]
2	$CH_5^+ + CH \rightarrow CH_2^+ + CH_4$	6.90E-10			[10]
3	$CH_5^+ + C \rightarrow CH^+ + CH_4$	1.20E-09			[10]
4	$CH_5^+ + C_2H_6 \rightarrow C_2H_5^+ + H_2 + CH_4$	2.25E-10			[10]
5	$CH_5^+ + C_2H_4 \rightarrow C_2H_5^+ + CH_4$	1.50E-09			[10]
6	$CH_5^+ + C_2H_2 \rightarrow C_2H_3^+ + CH_4$	1.60E-09			[10]
7	$CH_5^+ + C_2H \rightarrow C_2H_2^+ + CH_4$	9.00E-10			[10]
8	$CH_5^+ + C_2 \rightarrow C_2H^+ + CH_4$	9.50E-10			[10]
9	$CH_5^+ + H \rightarrow CH_4^+ + H_2$	1.50E-10			[10]
10	$CH_4^+ + CH_4 \rightarrow CH_5^+ + CH_3$	1.50E-09			[10]
11	$CH_4^+ + C_2H_6 \rightarrow C_2H_4^+ + CH_4 + H_2$	1.91E-09			[10]
12	$CH_4^+ + C_2H_4 \rightarrow C_2H_5^+ + CH_3$	4.23E-10			[10]

(*continued on next page*)

Table A5 – (*continued*)

No.	Reaction	A	*n*	E/R	Ref.
13	$CH_4^+ + C_2H_4 \rightarrow C_2H_4^+ + CH_4$	1.38E-09			[10]
14	$CH_4^+ + C_2H_2 \rightarrow C_2H_3^+ + CH_3$	1.23E-09			[10]
15	$CH_4^+ + C_2H_2 \rightarrow C_2H_2^+ + CH_4$	1.13E-09			[10]
16	$CH_4^+ + H_2 \rightarrow CH_5^+ + H$	3.30E-11			[10]
17	$CH_4^+ + H \rightarrow CH_3^+ + H_2$	1.00E-11			[10]
18	$CH_3^+ + CH_4 \rightarrow CH_4^+ + CH_3$	1.36E-10			[10]
19	$CH_3^+ + CH_4 \rightarrow C_2H_5^+ + H_2$	1.20E-09			[10]
20	$CH_3^+ + CH_2 \rightarrow C_2H_3^+ + H_2$	9.90E-10			[10]
21	$CH_3^+ + CH \rightarrow C_2H_2^+ + H_2$	7.10E-10			[10]
22	$CH_3^+ + C \rightarrow C_2H^+ + H_2$	1.20E-09			[10]
23	$CH_3^+ + C_2H_6 \rightarrow C_2H_5^+ + CH_4$	1.48E-09			[10]
24	$CH_3^+ + C_2H_4 \rightarrow C_2H_3^+ + CH_4$	3.50E-10			[10]
25	$CH_3^+ + C_2H_3 \rightarrow C_2H_3^+ + CH_3$	3.00E-10			[10]
26	$CH_2^+ + CH_4 \rightarrow CH_3^+ + CH_3$	1.38E-10			[10]
27	$CH_2^+ + CH_4 \rightarrow C_2H_5^+ + H$	3.60E-10			[10]
28	$CH_2^+ + CH_4 \rightarrow C_2H_4^+ + H_2$	8.40E-10			[10]
29	$CH_2^+ + CH_4 \rightarrow C_2H_3^+ + H_2 + H$	2.31E-10			[10]
30	$CH_2^+ + CH_4 \rightarrow C_2H_2^+ + H_2 + H_2$	3.97E-10			[10]
31	$CH_2^+ + C \rightarrow C_2H^+ + H$	1.20E-09			[10]
32	$CH_2^+ + H_2 \rightarrow CH_3^+ + H$	1.60E-09			[10]
33	$CH^+ + CH_4 \rightarrow C_2H_4^+ + H$	6.50E-11			[10]
34	$CH^+ + CH_4 \rightarrow C_2H_3^+ + H_2$	1.09E-09			[10]
35	$CH^+ + CH_4 \rightarrow C_2H_2^+ + H_2 + H$	1.43E-10			[10]
36	$CH^+ + CH_2 \rightarrow C_2H^+ + H_2$	1.00E-09			[10]
37	$CH^+ + CH \rightarrow C_2^+ + H_2$	7.40E-10			[10]
38	$CH^+ + C \rightarrow C_2^+ + H$	1.20E-09			[10]
39	$CH^+ + H_2 \rightarrow CH_2^+ + H$	1.20E-09			[10]
40	$CH^+ + H \rightarrow C^+ + H_2$	7.50E-10			[10]
41	$C^+ + CH_4 \rightarrow C_2H_3^+ + H$	1.10E-09			[10]
42	$C^+ + CH_4 \rightarrow C_2H_2^+ + H_2$	4.00E-10			[10]
43	$C^+ + CH_3 \rightarrow C_2H_2^+ + H$	1.30E-09			[10]
44	$C^+ + CH_3 \rightarrow C_2H^+ + H_2$	1.00E-09			[10]
45	$C^+ + CH_2 \rightarrow CH_2^+ + C$	5.20E-10			[10]
46	$C^+ + CH_2 \rightarrow C_2H^+ + H$	5.20E-10			[10]
47	$C^+ + CH \rightarrow CH^+ + C$	3.80E-10			[10]
48	$C^+ + CH \rightarrow C_2^+ + H$	3.80E-10			[10]
49	$C^+ + C_2H_6 \rightarrow C_2H_5^+ + CH$	2.31E-10			[10]
50	$C^+ + C_2H_6 \rightarrow C_2H_4^+ + CH_2$	1.16E-10			[10]
51	$C^+ + C_2H_6 \rightarrow C_2H_3^+ + CH_3$	4.95E-10			[10]
52	$C^+ + C_2H_6 \rightarrow C_2H_2^+ + CH_4$	8.25E-11			[10]
53	$C^+ + C_2H_5 \rightarrow C_2H_5^+ + C$	5.00E-10			[10]
54	$C^+ + C_2H_4 \rightarrow C_2H_4^+ + C$	1.70E-11			[10]
55	$C^+ + C_2H_4 \rightarrow C_2H_3^+ + CH$	8.50E-11			[10]
56	$C^+ + H^- \rightarrow C + H$	2.30E-07			[10]
57	$C_2H_6^+ + C_2H_4 \rightarrow C_2H_4^+ + C_2H_6$	1.15E-09			[10]
58	$C_2H_6^+ + C_2H_2 \rightarrow C_2H_5^+ + C_2H_3$	2.47E-10			[10]
59	$C_2H_6^+ + H \rightarrow C_2H_5^+ + H_2$	1.00E-10			[10]
60	$C_2H_5^+ + H \rightarrow C_2H_4^+ + H_2$	1.00E-11			[10]
61	$C_2H_4^+ + C_2H_3 \rightarrow C_2H_5^+ + C_2H_2$	5.00E-10			[10]
62	$C_2H_4^+ + C_2H_3 \rightarrow C_2H_3^+ + C_2H_4$	5.00E-10			[10]
63	$C_2H_4^+ + H \rightarrow C_2H_3^+ + H_2$	3.00E-10			[10]
64	$C_2H_3^+ + C_2H_6 \rightarrow C_2H_5^+ + C_2H_4$	2.91E-10			[10]
65	$C_2H_3^+ + C_2H_4 \rightarrow C_2H_5^+ + C_2H_2$	8.90E-10			[10]
66	$C_2H_3^+ + C_2H_3 \rightarrow C_2H_5^+ + C_2H$	5.00E-10			[10]
67	$C_2H_3^+ + C_2H \rightarrow C_2H_2^+ + C_2H_2$	3.30E-10			[10]
68	$C_2H_3^+ + H \rightarrow C_2H_2^+ + H_2$	6.80E-11			[10]
69	$C_2H_2^+ + CH_4 \rightarrow C_2H_3^+ + CH_3$	4.10E-09			[10]
70	$C_2H_2^+ + C_2H_6 \rightarrow C_2H_5^+ + C_2H_3$	1.31E-10			[10]
71	$C_2H_2^+ + C_2H_6 \rightarrow C_2H_4^+ + C_2H_4$	2.48E-10			[10]
72	$C_2H_2^+ + C_2H_4 \rightarrow C_2H_4^+ + C_2H_2$	4.14E-10			[10]
73	$C_2H_2^+ + C_2H_3 \rightarrow C_2H_3^+ + C_2H_2$	3.30E-10			[10]
74	$C_2H_2^+ + H_2 \rightarrow C_2H_3^+ + H$	1.00E-11			[10]
75	$C_2H^+ + CH_4 \rightarrow C_2H_2^+ + CH_3$	3.74E-10			[10]
76	$C_2H^+ + CH_2 \rightarrow CH_3^+ + C_2$	4.40E-10			[10]

Table A5 – (*continued*)

No.	Reaction	A	*n*	E/R	Ref.
77	$C_2H^+ + CH \rightarrow CH_2^+ + C_2$	3.20E-10			[10]
78	$C_2H^+ + H_2 \rightarrow C_2H_2^+ + H$	1.10E-09			[10]
79	$C_2^+ + CH_4 \rightarrow C_2H_2^+ + CH_2$	1.82E-10			[10]
80	$C_2^+ + CH_4 \rightarrow C_2H^+ + CH_3$	2.38E-10			[10]
81	$C_2^+ + CH_2 \rightarrow CH_2^+ + C_2$	4.50E-10			[10]
82	$C_2^+ + CH \rightarrow CH^+ + C_2$	3.20E-10			[10]
83	$C_2^+ + H_2 \rightarrow C_2H^+ + H$	1.10E-09			[10]
84	$H_3^+ + CH_4 \rightarrow CH_5^+ + H_2$	2.40E-09			[10]
85	$H_3^+ + CH_3 \rightarrow CH_4^+ + H_2$	2.10E-09			[10]
86	$H_3^+ + CH_2 \rightarrow CH_3^+ + H_2$	1.70E-09			[10]
87	$H_3^+ + CH \rightarrow CH_2^+ + H_2$	1.20E-09			[10]
88	$H_3^+ + C \rightarrow CH^+ + H_2$	2.00E-09			[10]
89	$H_3^+ + C_2H_6 \rightarrow C_2H_5^+ + H_2 + H_2$	2.40E-09			[10]
90	$H_3^+ + C_2H_5 \rightarrow C_2H_6^+ + H_2$	1.40E-09			[10]
91	$H_3^+ + C_2H_4 \rightarrow C_2H_5^+ + H_2$	1.15E-09			[10]
92	$H_3^+ + C_2H_4 \rightarrow C_2H_3^+ + H_2 + H_2$	1.15E-09			[10]
93	$H_3^+ + C_2H_3 \rightarrow C_2H_4^+ + H_2$	2.00E-09			[10]
94	$H_3^+ + C_2H_2 \rightarrow C_2H_3^+ + H_2$	3.50E-09			[10]
95	$H_2^+ + CH_4 \rightarrow CH_5^+ + H$	1.14E-10			[10]
96	$H_2^+ + CH_4 \rightarrow CH_4^+ + H_2$	1.40E-09			[10]
97	$H_2^+ + CH_4 \rightarrow CH_3^+ + H_2 + H$	2.30E-09			[10]
98	$H_2^+ + CH_2 \rightarrow CH_3^+ + H$	1.00E-09			[10]
99	$H_2^+ + CH_2 \rightarrow CH_2^+ + H_2$	1.00E-09			[10]
100	$H_2^+ + CH \rightarrow CH_2^+ + H$	7.10E-10			[10]
101	$H_2^+ + CH \rightarrow CH^+ + H_2$	7.10E-10			[10]
102	$H_2^+ + C \rightarrow CH^+ + H$	2.40E-09			[10]
103	$H_2^+ + C_2H_6 \rightarrow C_2H_6^+ + H_2$	2.94E-10			[10]
104	$H_2^+ + C_2H_6 \rightarrow C_2H_5^+ + H_2 + H$	1.37E-09			[10]
105	$H_2^+ + C_2H_6 \rightarrow C_2H_4^+ + H_2 + H_2$	2.35E-09			[10]
106	$H_2^+ + C_2H_6 \rightarrow C_2H_3^+ + H_2 + H_2 + H$	6.86E-10			[10]
107	$H_2^+ + C_2H_6 \rightarrow C_2H_2^+ + H_2 + H_2 + H_2$	1.96E-10			[10]
108	$H_2^+ + C_2H_4 \rightarrow C_2H_4^+ + H_2$	2.21E-09			[10]
109	$H_2^+ + C_2H_4 \rightarrow C_2H_3^+ + H_2 + H$	1.81E-09			[10]
110	$H_2^+ + C_2H_4 \rightarrow C_2H_2^+ + H_2 + H_2$	8.82E-10			[10]
111	$H_2^+ + C_2H_2 \rightarrow C_2H_3^+ + H$	4.80E-10			[10]
112	$H_2^+ + C_2H_2 \rightarrow C_2H_2^+ + H_2$	4.82E-09			[10]
113	$H_2^+ + C_2H \rightarrow C_2H_2^+ + H$	1.00E-09			[10]
114	$H_2^+ + C_2H \rightarrow C_2H^+ + H_2$	1.00E-09			[10]
115	$H_2^+ + C_2 \rightarrow C_2H^+ + H$	1.10E-09			[10]
116	$H_2^+ + C_2 \rightarrow C_2^+ + H_2$	1.10E-09			[10]
117	$H_2^+ + H_2 \rightarrow H_2 + H^+ + H$	1.00E-08		84,100	[43]
118	$H_2^+ + H \rightarrow H_3^+ + H$	2.10E-09			[43]
119	$H_2^+ + H \rightarrow H_2 + H^+$	6.39E-10			[43]
120	$H_2^+ + N \rightarrow N^+ + H_2$	5.00E-10			[43]
121	$H^+ + CH_4 \rightarrow CH_4^+ + H$	1.50E-09			[10]
122	$H^+ + CH_4 \rightarrow CH_3^+ + H_2$	2.30E-09			[10]
123	$H^+ + CH_3 \rightarrow CH_3^+ + H$	3.40E-09			[10]
124	$H^+ + CH_2 \rightarrow CH_2^+ + H$	1.40E-09			[10]
125	$H^+ + CH_2 \rightarrow CH^+ + H_2$	1.40E-09			[10]
126	$H^+ + CH \rightarrow CH^+ + H$	1.90E-09			[10]
127	$H^+ + C_2H_6 \rightarrow C_2H_5^+ + H_2$	1.30E-09			[10]
128	$H^+ + C_2H_6 \rightarrow C_2H_4^+ + H_2 + H$	1.40E-09			[10]
129	$H^+ + C_2H_6 \rightarrow C_2H_3^+ + H_2 + H_2$	2.80E-09			[10]
130	$H^+ + C_2H_5 \rightarrow C_2H_4^+ + H_2$	1.65E-09			[10]
131	$H^+ + C_2H_5 \rightarrow C_2H_3^+ + H_2 + H$	3.06E-09			[10]
132	$H^+ + C_2H_4 \rightarrow C_2H_4^+ + H$	1.00E-09			[10]
133	$H^+ + C_2H_4 \rightarrow C_2H_3^+ + H_2$	3.00E-09			[10]
134	$H^+ + C_2H_4 \rightarrow C_2H_2^+ + H_2 + H$	1.00E-09			[10]
135	$H^+ + C_2H_3 \rightarrow C_2H_3^+ + H$	2.00E-09			[10]
136	$H^+ + C_2H_3 \rightarrow C_2H_2^+ + H_2$	2.00E-09			[10]
137	$H^+ + C_2H_2 \rightarrow C_2H_2^+ + H$	5.40E-10			[10]
138	$H^+ + C_2H \rightarrow C_2H^+ + H$	1.50E-09			[10]
139	$H^+ + C_2H \rightarrow C_2^+ + H_2$	1.50E-09			[10]
140	$H^+ + C_2 \rightarrow C_2^+ + H$	3.10E-09			[10]

(*continued on next page*)

Table A5 – (*continued*)

No.	Reaction	A	*n*	E/R	Ref.
141	$H^+ + H_2 + M \rightarrow H_3^+ + M$	1.50E-29			[43]
142	$H^+ + H + M \rightarrow H_2^+ + M$	1.00E-34			[43]
143	$H^+ + N \rightarrow N^+ + H$	5.00E-11			[43]
144	$H^- + CH_3 \rightarrow CH_4 + e^-$	1.00E-09			[10]
145	$H^- + CH_2 \rightarrow CH_3 + e^-$	1.00E-09			[10]
146	$H^- + CH \rightarrow CH_2 + e^-$	1.00E-10			[10]
147	$H^- + C \rightarrow CH + e^-$	1.00E-09			[10]
148	$H^- + C_2H \rightarrow C_2H_2 + e^-$	1.00E-09			[10]
149	$H^- + C_2 \rightarrow C_2H + e^-$	1.00E-09			[10]
150	$H^- + M \rightarrow H + e^- + M$	2.70E-10	0.50	5590	[43]
151	$H^- + H \rightarrow H_2 + e^-$	1.30E-09			[43]
152	$H^- + N \rightarrow NH + e^-$	1.00E-09			[43]
153	$N_4^+ + C_3H_8 \rightarrow C_2H_5^+ + CH_3 + N_2 + N_2$	6.70E-10			[33]
154	$N_4^+ + C_3H_8 \rightarrow C_2H_4^+ + CH_4 + N_2 + N_2$	4.30E-10			[33]
155	$N_4^+ + M \rightarrow N_2^+ + M + N_2$	2.50E-15			[43]
156	$N_4^+ + N \rightarrow N_2 + N_2 + N^+$	1.00E-11			[43]
157	$N_3^+ + NH_3 \rightarrow NH_3^+ + N + N_2$	2.10E-09			[42]
158	$N_3^+ + N \rightarrow N_2^+ + N_2$	6.60E-11			[43]
159	$N_3^+ + M \rightarrow M + N + N_2^+$	6.60E-11			[43]
160	$N_2^+ + C_3H_8 \rightarrow C_2H_5^+ + CH_3 + N_2$	3.90E-10			[33]
161	$N_2^+ + C_3H_8 \rightarrow C_2H_4^+ + CH_4 + N_2$	2.20E-10			[33]
162	$N_2^+ + C_3H_8 \rightarrow C_2H_3^+ + CH_3 + H_2 + N_2$	5.20E-10			[33]
163	$N_2^+ + NH_3 \rightarrow NH_3^+ + N_2$	1.90E-09			[42]
164	$N_2^+ + N_2 + M \rightarrow N_4^+ + M$	6.80E-29	−1.64		[43]
165	$N_2^+ + N \rightarrow N_2 + N^+$	7.20E-13	1.00		[43]
166	$N_2^+ + N + M \rightarrow M + N_3^+$	9.00E-30	1.00	−400	[43]
167	$N^+ + NH_3 \rightarrow NH_3^+ + N$	2.40E-09			[42]
168	$N^+ + N + M \rightarrow N_2^+ + M$	1.00E-29			[43]
169	$N^+ + N_2 \rightarrow N + N_2^+$	4.45E-10			[43]
170	$N^+ + N_2 + M \rightarrow N_3^+ + M$	9.00E-30		−400	[43]
171	$N^+ + H \rightarrow N + H^+$	2.00E-09			[43]
172	$N^+ + NH \rightarrow H + N_2^+$	3.70E-10			[43]
173	$NH_3^+ + NH_3 \rightarrow NH_4^+ + NH_2$	2.20E-09			[44]
174	$NH_3^+ + H_2 \rightarrow NH_4^+ + H$	4.00E-13			[44]
175	$NH_2^+ + NH_3 \rightarrow NH_3^+ + NH_2$	1.10E-09			[44]
176	$NH_2^+ + NH_3 \rightarrow NH_4^+ + NH$	1.10E-09			[44]
177	$NH_2^+ + H_2 \rightarrow NH_3^+ + H$	1.00E-09			[44]
178	$NH^+ + NH_3 \rightarrow NH_3^+ + NH$	1.80E-09			[44]
179	$NH^+ + NH_3 \rightarrow NH_4^+ + N$	6.00E-10			[44]
180	$NH^+ + NH_2 \rightarrow NH + NH_2^+$	1.80E-09			[44]

Table A6 – Excited–neutral reactions included in the model and the references where these data were adopted from. Reaction coefficients are given by the Arrhenius function: $k(T) = A\,(T/300\ K)^n \exp(-E/RT)$ where T is the gas mixture temperature (in K) and A is given in units of $cm^3\ s^{-1}$ for two-body collisions and in $cm^6\ s^{-1}$ for three-body collisions.

No.	Reaction	A	E/R	Ref.
1	$H_2(vib.) + N_2 \rightarrow H_2 + N_2$	1.00E-13		[43]
2	$H_2(vib.) + N \rightarrow H_2 + N$	1.00E-13		[43]
3	$H_2(vib.) + H_2 \rightarrow H_2 + H_2$	1.00E-13		[43]
4	$H_2(rot.) + N_2 \rightarrow H_2 + N_2$	1.00E-13		[43]
5	$H_2(rot.) + N \rightarrow H_2 + N$	1.00E-13		[43]
6	$H_2(rot.) + H_2 \rightarrow H_2 + H_2$	1.00E-13		[43]
7	$H_2^* + N_2 \rightarrow H_2 + N_2$	1.00E-13		[43]
8	$H_2^* + N \rightarrow H_2 + N$	1.00E-13		[43]
9	$H_2^* + H_2 \rightarrow H_2 + H_2$	1.00E-13		[43]
10	$H^* + N_2 \rightarrow H + N_2$	1.00E-13		[43]
11	$H^* + N \rightarrow H + N$	1.00E-13		[43]
12	$H^* + H_2 \rightarrow H + H_2$	1.00E-13		[43]
13	$N_2(a'^1) + CH_4 \rightarrow N_2 + C + H_2 + H_2$	3.00E-10		[38]
14	$N_2(A^3) + CH_4 \rightarrow N_2 + CH_3 + H$	1.50E-12		[38]
15	$N_2(a'^1) + CH_4 \rightarrow CH_3 + H + N_2$	3.00E-10		[33]
16	$N_2^* + CH_4 \rightarrow N_2 + CH_2 + H_2$	1.35E-13		[38]

Table A6 – (*continued*)

No.	Reaction	A	E/R	Ref.
17	$N_2^* + C_3H_8 \rightarrow C_3H_6 + H_2 + N_2$	1.30E-12		[33]
18	$N_2(a'^1) + C_3H_8 \rightarrow C_3H_6 + H_2 + N_2$	3.00E-10		[33]
19	$N_2^* + C_3H_6 \rightarrow C_3H_5 + H + N_2$	1.40E-10		[33]
20	$N_2(a'^1) + C_3H_6 \rightarrow C_3H_5 + H + N_2$	1.40E-10		[33]
21	$N_2^* + C_3H_6 \rightarrow C_2H_3 + CH_3 + N_2$	1.40E-10		[33]
22	$N_2(a'^1) + C_3H_6 \rightarrow C_2H_3 + CH_3 + N_2$	1.40E-10		[33]
23	$N_2^* + C_2H_6 \rightarrow C_2H_4 + H_2 + N_2$	1.80E-10	1980	[33]
24	$N_2(a'^1) + C_2H_6 \rightarrow C_2H_4 + H_2 + N_2$	5.00E-08	1980	[33]
25	$N_2^* + C_2H_4 \rightarrow C_2H_3 + H + N_2$	5.50E-11		[33]
26	$N_2(a'^1) + C_2H_4 \rightarrow C_2H_3 + H + N_2$	2.00E-10		[33]
27	$N_2^* + C_2H_4 \rightarrow C_2H_2 + H_2 + N_2$	5.50E-11		[33]
28	$N_2(a'^1) + C_2H_4 \rightarrow C_2H_2 + H_2 + N_2$	2.00E-10		[33]
29	$N_2^* + C_2H_2 \rightarrow C_2H + H + N_2$	2.00E-10		[33]
30	$N_2(a'^1) + C_2H_2 \rightarrow C_2H + H + N_2$	3.00E-10		[33]
31	$N_2^* + CH_3 \rightarrow N_2 + CH_2 + H$	1.00E-13		[38]
32	$N_2^* + H_2 \rightarrow N_2 + H_2$	2.10E-10		[43]
33	$N_2^* + H_2 \rightarrow N_2 + H + H$	3.80E-10	3500	[43]
34	$N_2(a'^1) + H_2 \rightarrow N_2 + H_2$	2.10E-10		[43]
35	$N_2^* + H \rightarrow N_2 + H$	2.10E-10		[43]
36	$N_2(a'^1) + H \rightarrow N_2 + H$	2.10E-10		[43]
37	$N_2^* + N_2(a'^1) \rightarrow N_4^+ + e^-$	9.00E-12		[43]
38	$N_2^* + N_2(a'^1) \rightarrow N_2^+ + N_2 + e^-$	1.00E-12		[43]
39	$N_2^* + N_2^* \rightarrow N_2 + N_2^*$	2.00E-12		[43]
40	$N_2(a'^1) + N_2(a'^1) \rightarrow N_4^+ + e^-$	1.00E-11		[43]
41	$N_2(a'^1) + N_2(a'^1) \rightarrow N_2^+ + N_2 + e^-$	5.00E-13		[43]
42	$N_2(a'^1) + N_2(a'^1) \rightarrow N_2 + N_2(a'^1)$	2.00E-12		[43]
43	$N_2^* + N_2 \rightarrow N_2 + N_2$	3.70E-16		[43]
44	$N_2(a'^1) + N_2 \rightarrow N_2 + N_2$	3.70E-16		[43]
45	$N_2^* + N \rightarrow N_2 + N$	2.00E-11		[43]
46	$N_2(a'^1) + N \rightarrow N_2 + N$	2.00E-11		[43]
47	$N_2^* + HCN \rightarrow N_2 + CN + H$	6.00E-12		[38]
48	$N_2(rot.) + N_2 \rightarrow N_2 + N_2$	1.00E-13		[43]
49	$N_2(rot.) + N \rightarrow N_2 + N$	1.00E-13		[43]
50	$N_2(rot.) + H_2 \rightarrow N_2 + H_2$	1.00E-13		[43]
51	$N_2(vib.) + N_2 \rightarrow N_2 + N_2$	1.00E-13		[43]
52	$N_2(vib.) + N \rightarrow N_2 + N$	1.00E-13		[43]
53	$N_2(vib.) + H_2 \rightarrow N_2 + H_2$	1.00E-13		[43]
54	$N^* + H_2 \rightarrow NH + H$	4.60E-11	880	[43]
55	$N^* + N_2^+ \rightarrow N^+ + N_2$	1.00E-10		[43]
56	$N^* + NH_3 \rightarrow NH + NH_2$	5.00E-11		[42]
57	$N^* + M \rightarrow N + M$	2.40E-14		[43]

REFERENCES

[1] Khilyuk LF, Chilingar GV, Robertson JO, Endres B. Chapter 16-typical composition of natural gases. Gas migration events preceding earthquakes. Gulf Professional Publishing; 2000. p. 238–47.

[2] NaturalGas.org [internet]. Overview of natural gas: background [about 1 screen]. Washington D.C.: Natural Gas Supply Association c2004–2010 [cited 2013 may 15]. Available from: http://naturalgas.org/overview/background.asp.

[3] Karavalakis G, Hajbabaei M, Durbin TD, Johnson KC, Zheng Z, Miller WJ. The effect of natural gas composition on the regulated emissions, gaseous toxic pollutants, and ultrafine particle number emissions from a refuse hauler vehicle. Energy 2013;50:280–91.

[4] Solomon S, Qin D, Manning M, Marquis M, Averyt K, Tignor MMB, et al., editors. Climate change 2007: the physical science basis. Contribution of working group I to the fourth assesment report of the intergovernmental panel on climate change. New York: Cambridge University Press; 2007.

[5] Lunsford JH. Catalytic conversion of methane to more useful chemicals and fuels: a challenge for the 21st century. Catal Today 2000;63:165–74.

[6] Ross JRH. Natural gas reforming and CO_2 mitigation. Catal Today 2005;100:151–8.

[7] Gutsol A, Rabinovich A, Fridman A. Combustion-assisted plasma in fuel conversion. J Phys D Appl Phys 2011;44:274001.

[8] Tao X, Bai M, Li X, Long H, Shang S, Yin Y, et al. CH_4–CO_2 reforming by plasma – challenges and opportunities. Prog Energ Combust 2011;37:113–24.

[9] Petitpas G, Rollier J, Darmon A, Gonzalez-Aguilar J, Metkemeijer R, Fulcheri L. A comparative study of non-thermal plasma assisted reforming technologies. Int J Hydrogen Energy 2007;32:2848–67.

[10] Snoeckx R, Aerts R, Tu X, Bogaerts A. Plasma-based dry reforming: a computational study ranging from nanoseconds to seconds timescale. J Phys Chem C 2013;117:4957–70.

[11] Zhang Y, Li Y, Wang Y, Liu C, Eliasson B. Plasma methane conversion in the presence of carbon dioxide using dielectric-barrier discharges. Fuel Process Technol 2003;83:101–9.

[12] Goujard V, Tatibouët J-M, Batiot-Dupeyrat C. Carbon dioxide reforming of methane using a dielectric barrier discharge reactor: effect of Helium Dilution and kinetic model. Plasma Chem Plasma Process 2011;31:315–25.
[13] Nozaki T, Goujard V, Yuzawa S, Moriyama S, Ağıral A, Okazaki K. Selective conversion of methane to synthetic fuels using dielectric barrier discharge contacting liquid film. J Phys D Appl Phys 2011;44:274010.
[14] Tu X, Whitehead JC. Plasma-catalytic dry reforming of methane in an atmospheric dielectric barrier discharge: understanding the synergistic effect at low temperature. Appl Catal B Environ 2012;125:439–48.
[15] Scarduelli G, Guella G, Ascenzi D, Tosi P. Synthesis of liquid organic compounds from CH_4 and CO_2 in a dielectric barrier discharge operating at atmospheric pressure. Plasma Process Polym 2011;8:25–31.
[16] Fidalgo B, Domínguez A, Pis J, Menéndez J. Microwave-assisted dry reforming of methane. Int J Hydrogen Energy 2008;33:4337–44.
[17] Kim T-S, Song S, Chun K-M, Lee SH. An experimental study of syn-gas production via microwave plasma reforming of methane, iso-octane and gasoline. Energy 2010;35:2734–43.
[18] Li D, Li X, Bai M, Tao X, Shang S, Dai X, et al. CO_2 reforming of CH_4 by atmospheric pressure glow discharge plasma: a high conversion ability. Int J Hydrogen Energy 2009;34:308–13.
[19] Yang Y. Methane conversion and reforming by nonthermal plasma on Pins. Ind Eng Chem Res 2002;41:5918–26.
[20] Beloqui Redondo A, Troussard E, Van Bokhoven J a. Non-oxidative methane conversion assisted by corona discharge. Fuel Process Technol 2012;104:265–70.
[21] Yao SL, Suzuki E, Meng N, Nakayama A. A high-efficiency reactor for the pulsed plasma conversion of methane. Plasma Chem Plasma Process 2002;22:225–37.
[22] Lee H, Sekiguchi H. Plasma–catalytic hybrid system using spouted bed with a gliding arc discharge: CH_4 reforming as a model reaction. J Phys D Appl Phys 2011;44:274008.
[23] Indarto A, Choi J, Lee H, Song H. Effect of additive gases on methane conversion using gliding arc discharge. Energy 2006;31:2986–95.
[24] Gallagher MJ, Geiger R, Polevich A, Rabinovich A, Gutsol A, Fridman A. On-board plasma-assisted conversion of heavy hydrocarbons into synthesis gas. Fuel 2010;89:1187–92.
[25] Putra AEE, Nomura S, Mukasa S, Toyota H. Hydrogen production by radio frequency plasma stimulation in methane hydrate at atmospheric pressure. Int J Hydrogen Energy 2012;37:16000–5.
[26] Yuan J, Zhong X, Tan S. Methane conversion in the presence of oxygen under low-temperature radio frequency plasma. J Nat Gas Chem 2010;19:605–10.
[27] Gaudernack B, Lynum S. Hydrogen from natural gas without release of CO_2 to the atmosphere. Int J Hydrogen Energy 1998;23:1087–93.
[28] Kogelschatz U. Dielectric-barrier discharges: their history, discharge physics, and industrial applications. Plasma Chem Plasma Process 2003;23:1–46.
[29] Aerts R, Tu X, De Bie C, Whitehead JC, Bogaerts A. An investigation into the dominant reactions for ethylene destruction in non-thermal atmospheric plasmas. Plasma Process Polym 2012;9:994–1000.
[30] De Bie C, Martens T, Van Dijk J, Paulussen S, Verheyde B, Corthals S, et al. Dielectric barrier discharges used for the conversion of greenhouse gases: modeling the plasma chemistry by fluid simulations. Plasma Sources Sci Technol 2011;20:024008.
[31] Chang MB, Balbach JH, Rood MJ, Kushner MJ. Removal of SO_2 from gas streams using a dielectric barrier discharge and combined plasma photolysis. J Appl Phys 1991;69:4409–17.
[32] Dorai R, Hassouni K, Kushner MJ. Interaction between soot particles and NO_x during dielectric barrier discharge plasma remediation of simulated diesel exhaust. J Appl Phys 2000;88:6060–71.
[33] Moreau N, Pasquiers S, Blin-Simiand N, Magne L, Jorand F, Postel C, et al. Propane dissociation in a non-thermal high-pressure nitrogen plasma. J Phys D Appl Phys 2010;43:285201.
[34] Koeta O, Blin-Simiand N, Faider W, Pasquiers S, Bary A, Jorand F. Decomposition of acetaldehyde in atmospheric pressure filamentary nitrogen plasma. Plasma Chem Plasma Process 2012;32:991–1023.
[35] Horvath G, Mason NJ, Polachova L, Zahoran M, Moravsky L, Matejcik S. Packed bed DBD discharge experiments in admixtures of N_2 and CH_4. Plasma Chem Plasma Process 2010;30:565–77.
[36] Legrand J, Diamy A, Hrach R, Hrachova V. Kinetics of reactions in CH_4/N_2 afterglow plasma. Vacuum 1997;48:671–5.
[37] Majumdar A, Behnke JF, Hippler R, Matyash K, Schneider R. Chemical reaction studies in CH_4/Ar and CH_4/N_2 gas mixtures of a dielectric barrier discharge. J Phys Chem A 2005;109:9371–7.
[38] Pintassilgo CD, Jaoul C, Loureiro J, Belmonte T, Czerwiec T. Kinetic modelling of a N_2 flowing microwave discharge with CH_4 addition in the post-discharge for nitrocarburizing treatments. J Phys D Appl Phys 2007;40:3620–32.
[39] Jauberteau JL, Jauberteau I, Cinelli MJ, Aubreton J. Reactivity of methane in a nitrogen discharge afterglow. New J Phys 2002;4:1–13.
[40] Savinov SY, Lee H, Keun H, Na B. The effect of vibrational excitation of molecules on plasmachemical reactions involving methane and nitrogen. Plasma Chem Plasma Process 2003;23:159–73.
[41] Legrand J, Diamy A, Hrach R, Hrachova V. Methane conversion in the flowing afterglow of a dinitrogen microwave plasma: initiation of the reaction. Contrib Plasma Phys 1997;37:521–37.
[42] Dorai R. Modeling of atmospheric pressure plasma processing of gases and surfaces. University of Illinois at Urbana-Champaign; 2002.
[43] Van Gaens W, Bogaerts A. Kinetic modelling for an atmospheric pressure argon plasma jet in humid air. J Phys D Appl Phys 2013;46:275201.
[44] Arakoni RA, Bhoj AN, Kushner MJ. H_2 generation in Ar/NH_3 microdischarges. J Phys D Appl Phys 2007;40:2476–90.
[45] Aerts R, Martens T, Bogaerts A. Influence of vibrational states on CO_2 splitting by dielectric barrier discharges. J Phys Chem C 2012;116:23257–73.
[46] Fridman A. Plasma chemistry. New York: Cambridge University Press; 2008.
[47] Gallon HJ. Dry reforming of methane using non-thermal plasma-catalysis. University of Manchester; 2010.
[48] Indarto A, Coowanitwong N, Choi J-W, Lee H, Song HK. Kinetic modeling of plasma methane conversion in a dielectric barrier discharge. Fuel Process Technol 2008;89:214–9.
[49] Thanyachotpaiboon K, Chavadej S, Caldwell TA, Lobban LL, Mallinson RG. Conversion of methane to higher hydrocarbons in AC nonequilibrium plasmas. AIChE J 1998;44:2252–7.
[50] GRI-Mech [internet]. Berkeley (CA): Gas Research Institute. [cited 2013 may 15]. Available from: http://www.me.berkeley.edu/gri_mech/index.html.